Deep-Sea Research II 139 (2017) 40–57

Contents lists available at ScienceDirect

Deep-Sea Research II

journal homepage: www.elsevier.com/locate/dsr2

Changing distributions of sea ice melt and meteoric water west of the Antarctic Peninsula

Michael P. Meredith [a,*], Sharon E. Stammerjohn [b], Hugh J. Venables [a], Hugh W. Ducklow [c], Douglas G. Martinson [c], Richard A. Iannuzzi [c], Melanie J. Leng [d,e], Jan Melchior van Wessem [f], Carleen H. Reijmer [f], Nicholas E. Barrand [g]

[a] British Antarctic Survey, Cambridge, UK
[b] Institute of Arctic and Alpine Research, University of Colorado, Boulder, CO, USA
[c] Lamont-Doherty Earth Observatory, Columbia University, New York, USA
[d] NERC Isotope Geosciences Facilities, British Geological Survey, Keyworth, UK
[e] Centre for Environmental Geochemistry, University of Nottingham, UK
[f] Institute for Marine and Atmospheric Research, Utrecht, Netherlands
[g] School of Geography, Earth and Environmental Sciences, University of Birmingham, UK

ARTICLE INFO

Available online 3 May 2016

Keywords:
Ocean–ice–atmosphere system
Meltwater
Ocean circulation
Sea ice
West Antarctic Peninsula

ABSTRACT

The Western Antarctic Peninsula has recently undergone rapid climatic warming, with associated decreases in sea ice extent and duration, and increases in precipitation and glacial discharge to the ocean. These shifts in the freshwater budget can have significant consequences on the functioning of the regional ecosystem, feedbacks on regional climate, and sea-level rise. Here we use shelf-wide oxygen isotope data from cruises in four consecutive Januaries (2011–2014) to distinguish the freshwater input from sea ice melt separately from that due to meteoric sources (precipitation plus glacial discharge). Sea ice melt distributions varied from minima in 2011 of around 0 % up to maxima in 2014 of around 4–5%. Meteoric water contribution to the marine environment is typically elevated inshore, due to local glacial discharge and orographic effects on precipitation, but this enhanced contribution was largely absent in January 2013 due to anomalously low precipitation in the last quarter of 2012. Both sea ice melt and meteoric water changes are seen to be strongly influenced by changes in regional wind forcing associated with the Southern Annular Mode and the El Niño–Southern Oscillation phenomenon, which also impact on net sea ice motion as inferred from the isotope data. A near-coastal time series of isotope data collected from Rothera Research Station reproduces well the temporal pattern of changes in sea ice melt, but less well the meteoric water changes, due to local glacial inputs and precipitation effects.

1. Introduction

The freshwater system of the Southern Ocean is a critical factor in determining the time-evolving ocean circulation and properties, and in structuring the marine ecosystem and its response to climatic change (e.g. Dierssen et al., 2002; Jullion et al., 2013; Rye et al., 2014). Partly this is a consequence of the very strong dependence of seawater density on salinity at low temperatures, with implications for geostrophic flows, stratification, mixing, and so on. Each of the contributors to the freshwater budget of the Southern Ocean (sea ice, glacial melt from Antarctica, iceberg calving and subsequent melt, precipitation) has the capacity to influence marine ecology and biodiversity, not only by shaping the physical environment, but also by influencing habitat suitability and the biogeochemistry of the marine system (Boyd and Ellwood, 2010; Ducklow et al., 2012; Raiswell, 2011; Venables et al., 2013).

Climatic change around Antarctica and the Southern Ocean is complex and spatially very heterogeneous (Turner et al., 2005). The most rapidly warming sector is West Antarctica, within which the Western Antarctic Peninsula (WAP) has been the fastest-warming region in the Southern Hemisphere (Vaughan et al., 2003). During the second half of the twentieth century, annual-mean atmospheric warming at WAP stations averaged 3.7 ± 1.6 °C/century, with the strongest warming occurring in the autumn and winter (Smith et al., 1996; Van Wessem et al., 2015; Vaughan et al., 2003).

At the WAP, sea ice is known to be especially significant in influencing local climate (King, 1994; Meredith and King, 2005). Unlike other sectors of Antarctica, the winds have a significant onshore component here, and hence air masses cross the sea ice

* Corresponding author.
E-mail address: mmm@bas.ac.uk (M.P. Meredith).

http://dx.doi.org/10.1016/j.dsr2.2016.04.019
0967-0645/

before encountering land (Harangozo, 2006; King and Harangozo, 1998). Consequently, the extent of sea ice adjacent to the WAP is a critical factor in determining local atmospheric temperatures (Smith and Stammerjohn, 2001; Turner et al., 2013). The ocean adjacent to the WAP has been marked by a rapid loss of sea ice in recent decades, comprised of a moderate trend toward earlier retreat in spring, coupled with a more pronounced trend toward later advance in autumn (Stammerjohn et al., 2008a).

Concurrent with the atmospheric warming, and strongly linked with the sea ice changes, the upper ocean at the WAP warmed significantly during the second half of the twentieth century (Meredith and King, 2005). It has also been shown that the delivery of heat to the WAP shelf via the intrusion of deep waters from the Antarctic Circumpolar Current (ACC) increased over similar timescales (Martinson, 2011a; Schmidtko et al., 2014). The ACC is the major oceanographic current system that inhabits the Southern Ocean; unlike other sectors, it lies immediately adjacent to the Antarctic shelf at the WAP, enabling the warm, saline waters from its mid-layers to intrude onto the shelf in relatively unmodified form (Klinck et al., 2004; Martinson et al., 2008).

In regions of West Antarctica that are exhibiting rapid loss of ice shelves, the warming and greater penetration of deep waters from the ACC onto and across the shelf has been invoked as the major proximal cause of the ice loss (Pritchard et al., 2012; Schmidtko et al., 2014). At the WAP, the role of atmospheric warming has also been implicated in glacial ice loss, since it is the one region of Antarctica where temperatures are sufficiently high to enable significant melt and runoff to occur (Vaughan et al., 2003). The annual duration of the melt season at the WAP has increased in recent decades, which is suggested to have contributed to ice shelf collapse (Scambos et al., 2000; van den Broeke, 2005) and the acceleration and thinning of glaciers (Pritchard and Vaughan, 2007) and although most of the meltwater will percolate down and refreeze within the firn layer, there is still the potential for an increase in runoff to the ocean (Barrand et al., 2013b; Vaughan, 2006). Overall, 80% of the glaciers at the WAP are known to have retreated during the second half of the twentieth century, with a recent tendency toward accelerated retreat (Cook et al., 2005). Recent modeling studies have suggested that the currently observed trends of glacier melting, recession and thinning are expected to continue at the peripheries of the Antarctic Peninsula (Davies et al., 2014), while the interior ice sheet may thicken in response to increased accumulation (Barrand et al., 2013a).

Discharge of ice from glaciers can be in the form of direct melt to the ocean, or via the calving of icebergs. The WAP is typically not characterized by the presence of large icebergs (> 18 km in length), though smaller icebergs are present due to local calving and advection into the region from other sectors. The distribution of these is such that the southern WAP shows greater volumes than the north (e.g. Fig. 9 of Tournadre et al., 2016).

Precipitation at the WAP is known to have increased in recent decades, with station data showing more precipitation events and an increasing tendency for rainfall rather than snowfall (Kirchgäßner, 2011; Turner et al., 1997). Shallow ice cores also indicate increasing precipitation over the last century, with a doubling inferred for some locations (Thomas et al., 2008).

Such changes in the freshwater system can have profound effects on the upper ocean at the WAP, and the regional ecosystem. One manifestation of this is the role of freshwater in stabilising the water column: a thin layer of ice melt will act to enhance stratification, and thus create an environment more favourable for phytoplankton blooms, whereas processes that reduce stratification (e.g. strong ice production in winter) can have the opposite effect (Dierssen et al., 2002; Mitchell and Holm-Hansen, 1991). In northern Marguerite Bay (adjacent to Adelaide Island; Fig. 1a), decreases in sea ice cover since 1998 have resulted in deeper winter mixed layers, and consequently reduced stratification and phytoplankton concentration in spring (Venables et al., 2013).

At Palmer Station (Anvers Island; Fig. 1a), positive anomalies in summer chlorophyll-a have been related to positive anomalies in the preceding winter sea ice extent followed by anomalously later ice edge retreats, weaker winds and less cloud cover in spring (Montes-Hugo et al., 2009; Saba et al., 2014). Years with positive chlorophyll-a anomalies were associated with the initiation of a robust cohort of krill the following summer, as evidenced in the diets of Adélie penguins (Saba et al., 2014). On the Peninsula scale, phytoplankton biomass along the WAP decreased overall since the late 1970s (Montes-Hugo et al., 2009) with strong negative trends occurring in the now mostly ice-free region north of 63°S (i.e., north of Palmer Station), concurrent with positive trends in the far southern region where the sea ice cover transitioned from quasi-perennial to seasonal.

Glacial discharge can also influence the WAP marine ecosystem due to the capacity of glaciers to supply micronutrients such as iron to the ocean, the low levels of which limit productivity across large regions of the open Southern Ocean away from such sources (Edwards and Sedwick, 2001; Raiswell, 2011). Scouring of the underlying rock and sediment, in addition to accumulation from atmospheric deposition, can result in glacial ice being significantly enriched in such micronutrients (Boyd and Ellwood, 2010). It has been suggested that an increase in freshwater input to the ocean from glaciers could result in a greater injection of such micronutrients (Hawkings et al., 2014), a shift in phytoplankton assemblage composition, and an increase in biomass in the waters influenced (Dierssen et al., 2002).

Understanding the full effects of these changes on the diverse aspects of the marine biogeochemical and biological systems requires detailed measurements that are very difficult to obtain on a circumpolar scale. A different approach to achieving progress is to study the system in a region of known rapid climate change, so that a mechanistic understanding can be developed, and can give insight into the future of other sectors as their climates evolve. Here, we explore in detail the time-varying freshwater distributions in a region of recent rapid change, and elucidate the processes responsible for the changes and their impacts.

2. Background

2.1. Water masses, circulation and variability at the WAP

The presence of the southern edge of the ACC adjacent to the WAP shelf leads to a northeastward flow along the shelf break. The mid-layer waters of the ACC, termed Circumpolar Deep Water (CDW) are consequently brought into close proximity with the shelf break, and the glacial canyons that dissect the shelf (Fig. 1a) provide efficacious conduits for the intrusion of this CDW and its flow toward land. Eddy dynamics are believed to be significant in these processes (Martinson, 2011b; Moffat et al., 2009). This CDW mixes upwards on the shelf, providing heat and macronutrients to the upper layers of the water column. The locations and processes that enable this mixing are thought to be heterogeneously distributed, with coastal upwelling and internal tides highlighted previously (Wallace et al., 2008).

In winter, the CDW is overlain by a thick (50–150 m) mixed layer with temperatures close to the freezing point and salinities up to 34.0 (Klinck, 1998; Meredith et al., 2004). In summer, the surface of this layer is warmed by insolation and freshened by ice melt, leading to the existence of a subsurface temperature-minimum layer termed Winter Water (WW; Mosby, 1934). The properties of the upper layers change markedly across the shelf,

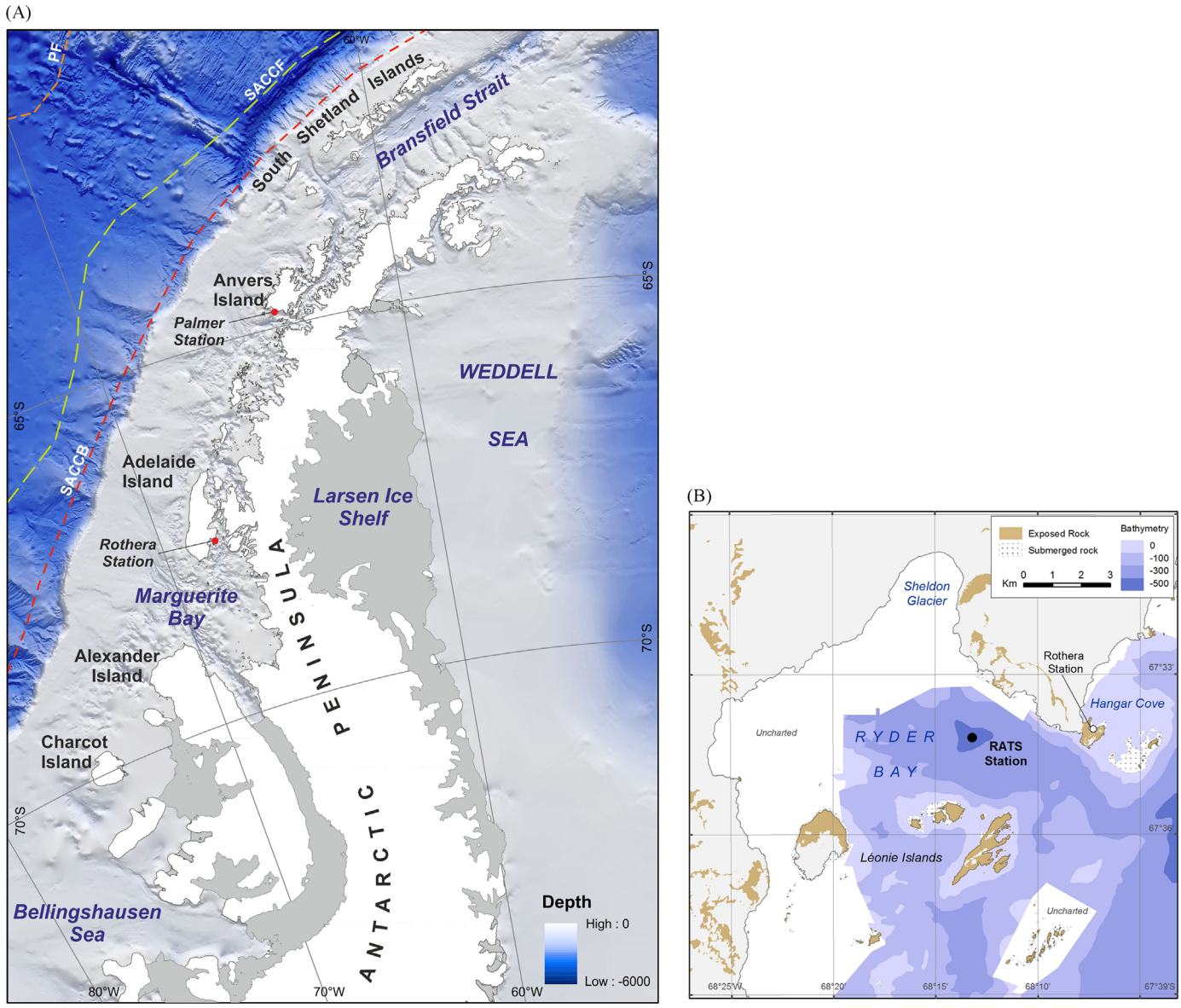

Fig. 1. (a) Bathymetry of Antarctic Peninsula shelf, with selected locations marked. Shown schematically are the fronts of the Antarctic Circumpolar Current (ACC) present in the vicinity, namely the Southern ACC Boundary (SACCB), Southern ACC Front (SACCF), and Polar Front (PF). (b) Locality of the Rothera Time Series (RaTS) sampling site in Ryder Bay, southeast Adelaide Island. Rothera Research Station is marked, as per (a).

due especially to lateral gradients in freshwater inputs and associated with the presence of a southwestward-flowing current in the near-shore regions. This has been termed the Antarctic Peninsula Coastal Current (APCC), the structure and transport of which was first documented by Moffat et al. (2008). The coherence of this current along the western edges of Adelaide Island and Alexander Island (Fig. 1a) is well established, but its circulation and variability within Marguerite Bay is not yet fully determined. The existence of cyclonic, semi-enclosed gyres separating the northeastward flow at the shelf break and the southwestward flow of the APCC has been postulated, though the structural persistence of such features has not been resolved in detail. Further information is presented in Beardsley et al. (2004), Klinck et al. (2004), Savidge and Amft (2009) etc., though in general the temporal variability of ocean circulation at the WAP is relatively poorly constrained

On interannual timescales, the major drivers of atmospheric variability at the WAP are the Southern Annular Mode (SAM) and the El Niño–Southern Oscillation (ENSO) phenomenon (Marshall et al., 2006; Meredith et al., 2008b; Stammerjohn et al., 2008b). SAM is characterized by meridional movements of atmospheric mass between a node over Antarctica and an annulus encircling the lower-latitude Southern Ocean (Thompson and Wallace, 2000). Accordingly, shifts in the strength of the circumpolar westerly winds over the Southern Ocean are closely linked to SAM, with variability occurring on timescales from weeks to decades. Whilst mostly zonal in form, SAM has significant meridional components, especially in and around the Amundsen-Bellingshausen Sea sector of the Southern Ocean. SAM has progressively moved to a more positive state in recent decades, due to a combination of natural variability and anthropogenic effects (stratospheric ozone depletion and/or radiative forcing from greenhouse gases (Marshall, 2003; Thompson et al., 2000)). Whilst SAM variability is intrinsically extra-tropical, ENSO variability is sourced in the equatorial Pacific region. However, this mode of climate variability has a marked impact on the southeast Pacific sector of the Southern Ocean via both atmospheric and oceanic

teleconnections (Meredith et al., 2008b; Turner, 2004; Yuan, 2004).

Both SAM and ENSO have pronounced impacts on the meridional winds and atmospheric temperatures at the WAP. During La Niña or positive SAM events, negative atmospheric pressure anomalies are typically present in the southeast Pacific, with the converse true for El Niño or negative SAM events. Cyclonic flow associated with the low pressure anomalies contributes to increased northerly winds over the WAP during La Niña and/or positive SAM conditions, with an associated increase in the delivery of warm, maritime air masses to the WAP. Conversely, anticyclonic flow associated with high pressure anomalies linked to El Niño and/or negative SAM conditions result in the greater local preponderance of colder, drier air masses. The coincident phasing of these two atmospheric modes can thus amplify or dampen the atmospheric circulation changes and climatic anomalies at the WAP (Clem and Fogt, 2013; Fogt and Bromwich, 2006; Stammerjohn et al., 2008b).

2.2. Oxygen isotope ratios as oceanographic tracers at the WAP

Measurements of salinity can be used to quantify the total freshwater added to a water parcel relative to a saline endmember, but do not provide information on the source of that freshwater *per se*. For this, an additional tracer is needed, and the ratio of oxygen isotopes in seawater ($\delta^{18}O$, the standardized ratio of $H_2{}^{18}O$ to $H_2{}^{16}O$) is extremely useful in this context. This tracer, when measured alongside salinity, enables the freshwater content of a water sample to be subdivided quantitatively into contributions from sea ice melt and meteoric water (i.e. water of meteorological origin, specifically precipitation and glacial discharge (Craig and Gordon, 1965)) due to their different isotope compositions. This difference in endmember $\delta^{18}O$ values is a consequence of high latitude precipitation being isotopically very light, whereas sea ice has similar $\delta^{18}O$ to the seawater from which it formed, which is much isotopically heavier. $\delta^{18}O$ has been used as a freshwater tracer at various locations around the Southern Ocean (e.g. Meredith et al., 1999; Schlosser et al., 1990; Weiss et al., 1979).

At the WAP, we have previously used time series measurements of $\delta^{18}O$ and salinity from a coastal site in northern Marguerite Bay (close to Rothera Research Station; Fig. 1a and b) to document seasonal (Meredith et al., 2008a) and interannual (Meredith et al., 2010) variability in the prevalence of sea ice melt and meteoric water. It was found that meteoric water dominated the freshwater budget overall, accounting for up to 5% of the water in the near-surface layer in summer, whereas seasonal variability in sea ice melt was found to be comparable to that of the meteoric water (around 1–2%) (Meredith et al., 2008a). On interannual timescales, variability in the freshwater fractions was found to be significantly influenced by climatic variability associated with both SAM and ENSO (Meredith et al., 2010).

To gain a larger-scale perspective on the spatial structure of the freshwater distribution, sampling was conducted on a research cruise in January 2011 that completed a grid of ocean stations across the WAP shelf between Anvers Island and Charcot Island (Figs. 1 and 2a; Meredith et al., 2013). This showed that meteoric water fractions were significantly elevated inshore on the WAP shelf (up to around 5% of the volume of the water, compared to

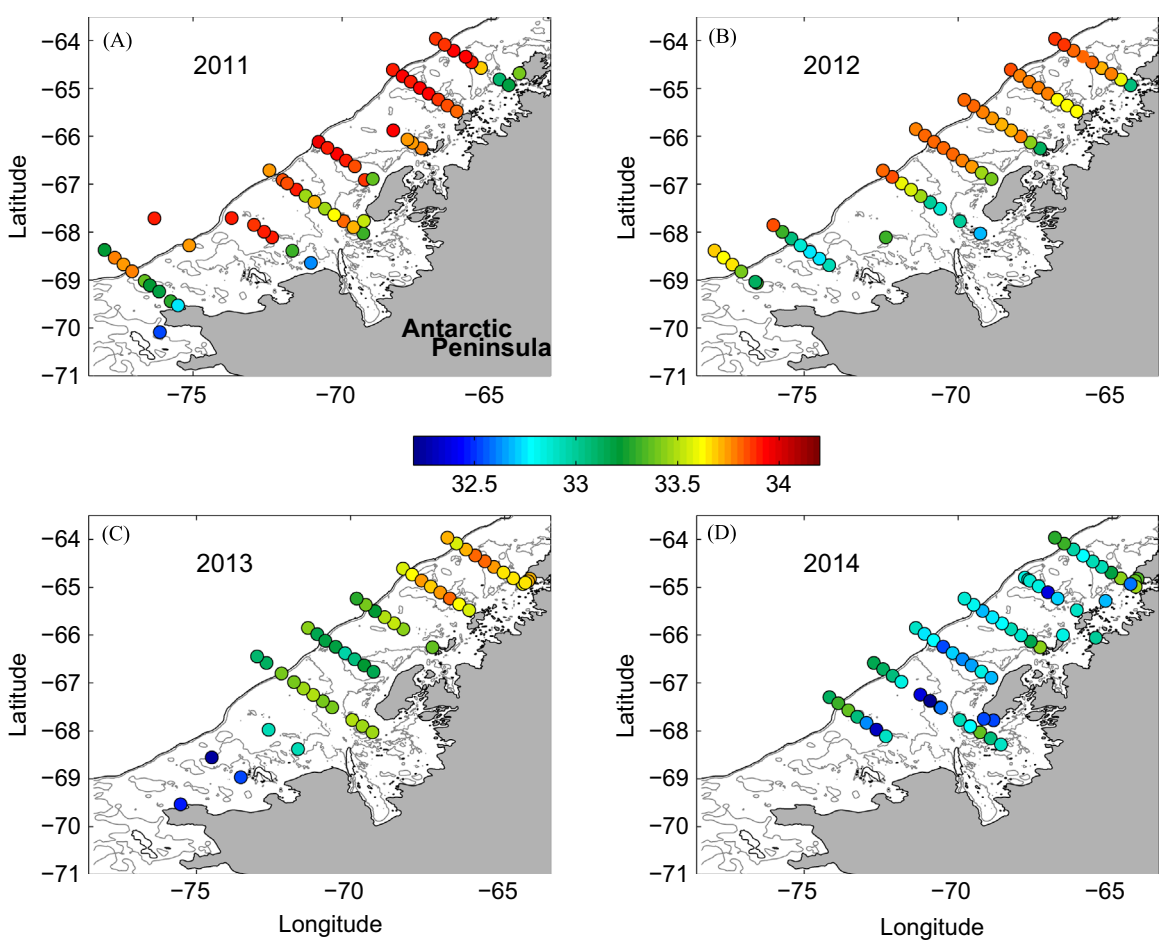

Fig. 2. Near-surface (upper 10 m) salinity distributions from Palmer LTER cruises in Januaries of (a) 2011, (b) 2012, (c) 2013 and (d) 2014. Data are from the upper bottles of CTD/Niskin casts and underway sampling events.

around 2% near the shelf edge); this was attributed to the stronger influence of glacial melt close to the glaciers themselves, combined with the orographic effects on precipitation induced by the mountains that form the spine of the Peninsula. The cross-shelf gradients in meteoric water were reflected in cross-shelf gradients in salinity, with implications for southward geostrophic flow in the inshore region.

Sea ice melt in January 2011 typically had much lower prevalence than meteoric water (around −1% to +1%, where a negative number denotes a net sea ice formation from that water prior to the time of sampling). It was observed that sea ice melt was much more heterogeneously distributed than meteoric water, attributable to the mobile nature of the sea ice. However, the data indicated sea ice production predominantly toward the northern end of the grid and sea ice melt predominantly toward the south, and thus a net southward sea ice transport that season was inferred (Meredith et al., 2013).

The near-shore time series data from Rothera show a long-term decrease in meteoric water in the near-surface layers since 2001, despite the known increases in glacial discharge and precipitation (Meredith et al., 2013). It has been shown that this decline in meteoric water is caused by a deepening of the mixed layer in winter, which has the effect of distributing the meteoric water over a greater vertical extent within the water column and thus diminishing its concentration near the surface. The mixed layer deepening is known to be a consequence of the reduction in sea ice close to Rothera, which leaves the ocean open to stronger wind-induced mixing and buoyancy losses in winter (Meredith et al., 2013).

Here, we extend the above studies by using cruise-based data from four consecutive years to provide unprecedented insight into the shelf-wide changes in freshwater distribution under time-varying forcings. This cruise-derived data are supplemented by the updated series from Rothera, which provides high temporal resolution sampling of the ocean and hence allows sub-annual timescales to be investigated contemporaneously.

3. Methods and data sources

3.1. Cruise-based sample collection

Discrete sampling for $\delta^{18}O$ was conducted from cruises undertaken by ARSV *Laurence M. Gould* at the WAP, as part of the Palmer Long-Term Ecological Research (Pal-LTER) programme (Ducklow et al., 2012). Four successive Januaries were sampled, covering the period 2011–2014. During each of these, samples were collected for isotope analysis from the underway water supply at 5 m depth. Additionally, samples were drawn from Niskin bottles closed at various depths during station-based profiling with a SeaBird 911*plus* conductivity–temperature–depth (CTD) instrument. The CTD salinity from the Pal-LTER cruises is accurate to around 0.002; the spatial pattern of samplings is shown in Fig. 2.

3.2. Time series sample collection

Sample collection was also conducted as part of the Rothera Oceanographic and Biological Time Series (RaTS; Clarke et al., 2008), which has been ongoing in Ryder Bay at Adelaide Island since 1997 (Fig. 1a and b). RaTS sampling includes quasi-weekly CTD profiling to 500 m depth with a SeaBird 19*plus* instrument, conducted from a rigid inflatable boat. Under fast ice conditions in winter, CTD profiling is conducted from sledge through a hole cut in the ice. At each RaTS sampling event, a Niskin bottle is lowered to 15 m depth and a water sample collected for determination of a range of variables, including salinity and $\delta^{18}O$. RaTS CTD data are calibrated using the discrete salinity measurements, and by concurrent profiling with the SeaBird 911*plus* on the ARSV *Laurence M. Gould* during the annual visits of the vessel to Rothera Research Station. Calibrated salinity from RaTS is accurate to better than 0.005.

3.3. Sample handling and measurement

Samples from RaTS were collected in 150 ml medical flat bottles with rubber inserts in the caps. These were then further sealed using Parafilm to prevent slippage of the cap and sample evaporation. Samples from Pal-LTER cruises were collected in 50 ml glass vials that were sealed with stoppers and aluminium crimps. All samples were transported by dark cool stow to the Natural Environment Research Council Isotope Geosciences Laboratory (NIGL) at the British Geological Survey, UK, for analysis using the equilibration method for oxygen (Epstein and Mayeda, 1953). Samples were analysed using an Isoprime mass spectrometer, and isotopic ratios are given as ‰ deviations from VSMOW2. Analytical reproducibility was <0.05‰ based on duplicate analyses.

3.4. Derivation of freshwater fractions

To quantitatively separate sea ice melt from meteoric water at the WAP, we use measurements of salinity and $\delta^{18}O$ to solve a simple 3-endmember mass balance, developed originally by Östlund and Hut (1984). At the WAP, this takes the form:

$$\begin{bmatrix} f_{sim}+f_{met}+f_{cdw}=1 \\ S_{sim}.f_{sim}+S_{met}.f_{met}+S_{cdw}.f_{cdw}=S \\ \delta_{sim}.f_{sim}+\delta_{met}.f_{met}+\delta_{cdw}.S_{cdw}=\delta \end{bmatrix} \quad (1)$$

where f_{sim}, f_{met} and f_{cdw} are, respectively, the fractions of sea ice melt, meteoric water and CDW that collectively constitute the water sample under consideration, which has salinity S and $\delta^{18}O$ value of δ. S_{sim}, S_{met} and S_{cdw} are the salinities of the pure components of sea ice melt, meteoric water and CDW, and δ_{sim}, δ_{met} and δ_{cdw} the corresponding $\delta^{18}O$ values of these components.

To enable comparison with previous studies, we here use the same endmember values as Meredith et al. (2013); these are given in Table 1. The availability of just two conservative freshwater tracers (salinity and $\delta^{18}O$) necessitates the choice of a single saline (oceanic) source, relative to which the freshwater fractions are derived. We use CDW for this, being the only water mass in the Southern Ocean with a net southward motion, hence all other waters circumpolarly are derived from this. (An alternative option is to adopt WW properties as the oceanic endmember, which inherently quantifies the freshening relative to the previous winter when the WW was formed, whereas using CDW inherently quantifies freshening relative to the most saline inflowing oceanic water in the region. This option was examined in detail by Meredith et al. (2013), who showed that the spatial fields obtained were almost identical to those obtained using CDW, just with smaller quantitative values). The salinity and $\delta^{18}O$ values chosen for the CDW endmember relate to a pure form of this water mass

Table 1
Endmember values used in the determination of freshwater fractions from combined salinity and oxygen isotope data (Eq. (1)). Full derivation of these endmembers is given in Meredith et al. (2013).

	Salinity	$\delta^{18}O$ (‰)
Sea ice melt	7	2.1
Meteoric water	0	−16
Circumpolar Deep Water	34.73	0.1

that intrudes onto the shelf, and are based upon various full-depth profiles of such parameters that have been obtained historically (Meredith et al., 2013, 2010).

The meteoric endmember is a combination of glacial melt and direct precipitation. The isotopic composition of each of these varies across the WAP region, and it is the uncertainty in the mean value of this endmember that introduces the greatest uncertainty in the final derived freshwater fractions. The value adopted here (−16‰) is the one derived by Meredith et al. (2010) based upon ice cores in the WAP region and consideration of direct measurements of isotopes in precipitation. Salinity of the meteoric water endmember is defined as zero. The endmember properties of sea ice are taken from historical measurements across the WAP region, and are discussed in Meredith et al. (2013).

To determine overall uncertainties in the derived freshwater fractions, sensitivity studies are conducted in which the mean value for each of the endmembers is adjusted within its individual uncertainty in Eq. (1) (Meredith et al., 2013). Overall, uncertainties better than 1% are obtained. This could be improved in future by better constraining the meteoric endmember, ideally by incorporating an extra tracer that could quantify precipitation separately from glacial discharge. At present, such data are not available, however.

3.5. RACMO

Modelled precipitation fields from the Regional Atmospheric Climate Model (RACMO2.3) (Van Wessem et al., 2015) are used for the study period (2011–2014). RACMO2.3 has been specifically adapted for use over glaciated regions such as Antarctica (e.g. Reijmer et al., 2005), and is applied to a domain encompassing the Antarctic Peninsula at a horizontal resolution of 5.5 km and with 40 vertical model levels. At the lateral boundaries the model is forced by ERA-Interim reanalysis data (January 1979–December 2014; Dee et al., 2011) and the interior of the domain is allowed to evolve freely. RACMO2.3 has been proven to realistically simulate Antarctic surface mass balance and implicitly the precipitation fields (Van Wessem et al., 2014), as well as the very large precipitation gradients along the coastal margins of the ice sheet.

3.6. Climatic data

Daily and monthly sea ice concentrations are from Version 2 of the Goddard Space Flight Center (GSFC) Bootstrap Scanning Multichannel Microwave Radiometer-Special Sensor Microwave/Imager (SMMR-SSM/I) time series (Comiso, 2002; Comiso and Nishio, 2008), augmented with Near Real Time Sea Ice daily data for 2014 (Maslanik and Stroeve, 1999) to produce a time series extending from 1979 to 2014. These data were provided by the EOS Distributed Active Archive Center (DAAC) at the National Snow and Ice Data Center (NSIDC, University of Colorado at Boulder, http://nsidc.org). We also determined monthly sea ice extent (total area inside the ice edge, the latter defined as the 15% sea ice concentration contour) for the WAP region, here defined as the area extending from the western coast of the Antarctic Peninsula to 80°W. (See Comiso and Nishio, 2008 for an explanation of the 15% threshold in determining sea ice extent.)

Using the daily sea ice concentrations, we identified the day of annual ice edge advance and retreat for each gridded (25×25 km^2 pixel) location and for each sea ice year that begins/ends during the mean summer sea ice minimum (mid-February) to obtain a time series of sea ice advance and retreat over 1979–1980 to 2013–2014 (methods described in Stammerjohn et al., 2008a). From this, we determined winter ice season duration (the time elapsed between the autumn advance and its subsequent spring retreat) at each gridded location. We show time series of ice season duration for three island areas (Anvers, Adelaide and Charcot), determined as spatial averages of areas approximately 200 km by 200 km adjacent to the islands.

Numerically-analysed monthly data of 10-m winds are from the European Centre for Medium Range Weather Forecasts (ECMWF) Interim Reanalysis (ERA-I) (Dee et al., 2011). Comparisons with sea-level pressure data from drifting ice buoys in the Bellingshausen Sea showed ERA-I to be the most accurate in capturing individual weather systems (as compared with other reanalysis products) on these spatial and temporal scales (Bracegirdle, 2013).

The SAM index used here is that of Marshall (2003), available at http://www.nerc-bas.ac.uk/icd/gjma/sam.html. For ENSO, the Niño3.4 index of Cane et al. (1986) was obtained from http://iridl.ldeo.columbia.edu and consists of sea surface temperatures averaged over 5°N to 5°S and 120–170°W. WAP sea level pressures extracted from ERA-I reanalysis were averaged over the region 60–70°S and 65–100°W.

Following the approach of Vaughan (2006) and Barrand et al. (2013b), station temperature time-series were processed to calculate annual positive degree day (PDD) sums. The PDD sum comprises the integral in kelvin days to January 15 each year of the excess of temperature above the melting point, 273.15 K, or 0 °C. Rather than the full summer season, this date was chosen to coincide with the timing of cruise data collection. Inclusive of the 2014 melt season, data from verified, shielded temperature sensors at the highest available temporal resolution (usually hourly) were used, and records missing more than a total of 7 days in any given melt season were discarded.

4. Freshwater distributions from oxygen isotope data

4.1. Near-surface salinity distributions

The near-surface (upper 10 m) distributions of salinity in each of the 4 years sampled are shown in Fig. 2. Note that Fig. 2a shows data already presented in Meredith et al. (2013). Whilst the southerly extent of the cruises varies between years due to the extent/concentration of sea ice presence at the time, the overlapping sections of data show significant interannual changes in salinity, and, by extension, total freshwater content.

The most saline year sampled was 2011, with salinities around 33.8–33.9 across much of the shelf in the northern part. Inshore of this region, salinities become markedly fresher toward land, dropping to approximately 33.2 in the vicinities of Anvers Island and Adelaide Island, and down to around 32.6–32.7 close to Alexander Island and Charcot Island.

In January 2012 (Fig. 2b), the spatial pattern of salinity was broadly similar to that observed in January 2011, in that salinities were generally lower toward the coast compared with offshore, especially across the northern part of the sampling grid. Salinities were generally lower in 2012, especially around Adelaide Island, though sparser near-shore sampling in the southern part of the region precludes comparison of salinity in the immediate vicinities of Alexander or Charcot Island.

The surface salinity distribution in January 2013 (Fig. 2c) differs quite markedly from the previous two years. Salinities were very much lower (around 33.2–33.3 across most of the grid, rising to 33.7 at the northern end and falling to 32.4 at the southern end), and the inshore decrease in salinity was notably absent.

In January 2014 (Fig. 2d), salinities had decreased still further, generally lying in the range 32.5–33.0 across most of the grid. There was only sparse evidence for nearshore decreases in salinity, though markedly low values were observed in the region around southern Adelaide Island.

4.2. Near-surface $\delta^{18}O$ distributions

In January 2011 (Fig. 3a), $\delta^{18}O$ values were around −0.4‰ to −0.35‰ across most of the WAP shelf, falling to around −0.6‰ close to land. General $\delta^{18}O$ values across much of the northern part of the sampling grid were similar in January 2012 to January 2011 (Fig. 3b; cf. Fig. 3a) being around −0.4‰. There is less evidence for inshore decreases in January 2012 in the northern end of the grid, however the southern end shows isotopically light waters (around −0.6‰ to −0.5‰) across much of its area.

By comparison, the WAP shelf waters in January 2013 (Fig. 3c) were isotopically heavy compared with 2011 and 2012, being typically around −0.4‰ to −0.35‰ over most of the northern part of the sampling area, though with significantly isotopically lighter waters in the southern part. In 2013, there is no evidence for inshore waters being isotopically lighter than those offshore, resembling strongly the distribution of salinity.

By January 2014, the feature of nearshore waters being isotopically lighter compared with those offshore is re-established, typically around −0.5‰ close to land versus −0.4‰ to −0.35‰ closer to the shelf edge. Noticeably isotopically light water was present around the southern edge of Adelaide Island (−0.6‰ to −0.55‰).

4.3. Near-surface sea ice melt distributions

The progression of sea ice melt across the 4 years (Fig. 4) reveals the lowest values in January 2011, when sea ice melt was in the range −1% to +1% across nearly all the sampling grid, and the highest values in January 2014 when sea ice melt was around 3–4% across much of the area. January 2012 (Fig. 4b) had values that were slightly higher than 2011, with increases in sea ice melt close to Anvers and Adelaide Islands, and at the southern end of the area. In January 2013, sea ice melt was typically in the range 0.5–2% across the whole area, with highest percentages in the middle sector.

4.4. Near-surface meteoric water distributions

As observed previously (Meredith et al., 2013), the meteoric water percentages in January 2011 were generally elevated inshore (Fig. 5a) relative to those offshore, and this was interpreted in terms of glacial discharge and enhanced precipitation due to orographic effects close to the coastal region. Within this overall spatial pattern, markedly high meteoric water concentrations (around 4–5%) were found near Anvers, Adelaide, Alexander and Charcot Islands. The first three of these local extremes were attributed to nearby strong glacial discharges, whereas that near Charcot Island was hypothesized to be due either to the southward transport of fresh, isotopically light waters that had been discharged along the length of the WAP, or to the relatively recent collapse of ice shelf features in that area.

In January 2012, meteoric water remained relatively low across most of the northern sector of the sampling grid, with values around 2–3% (Fig. 5b). Inshore and further south, values were higher, at around 3.5–4%. The following year (Fig. 5c), meteoric waters were again more prevalent at the southern end of the grid (up to 4–5% near Alexander and Charcot Islands), and were notably lower (2–3%) across the WAP shelf between Anvers and Adelaide Islands. In this sector of the shelf, there was no elevated meteoric

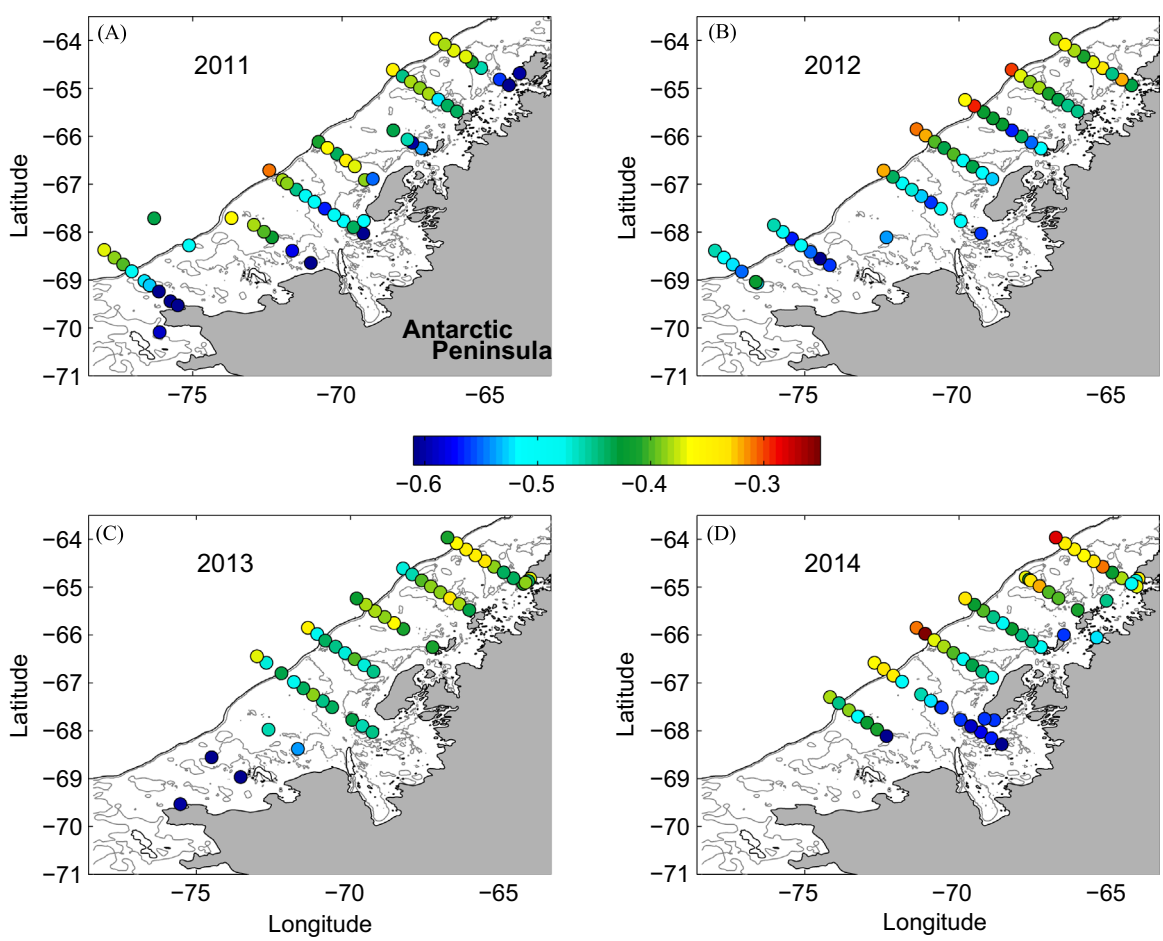

Fig. 3. As per Fig. 2, but for distributions of $\delta^{18}O$.

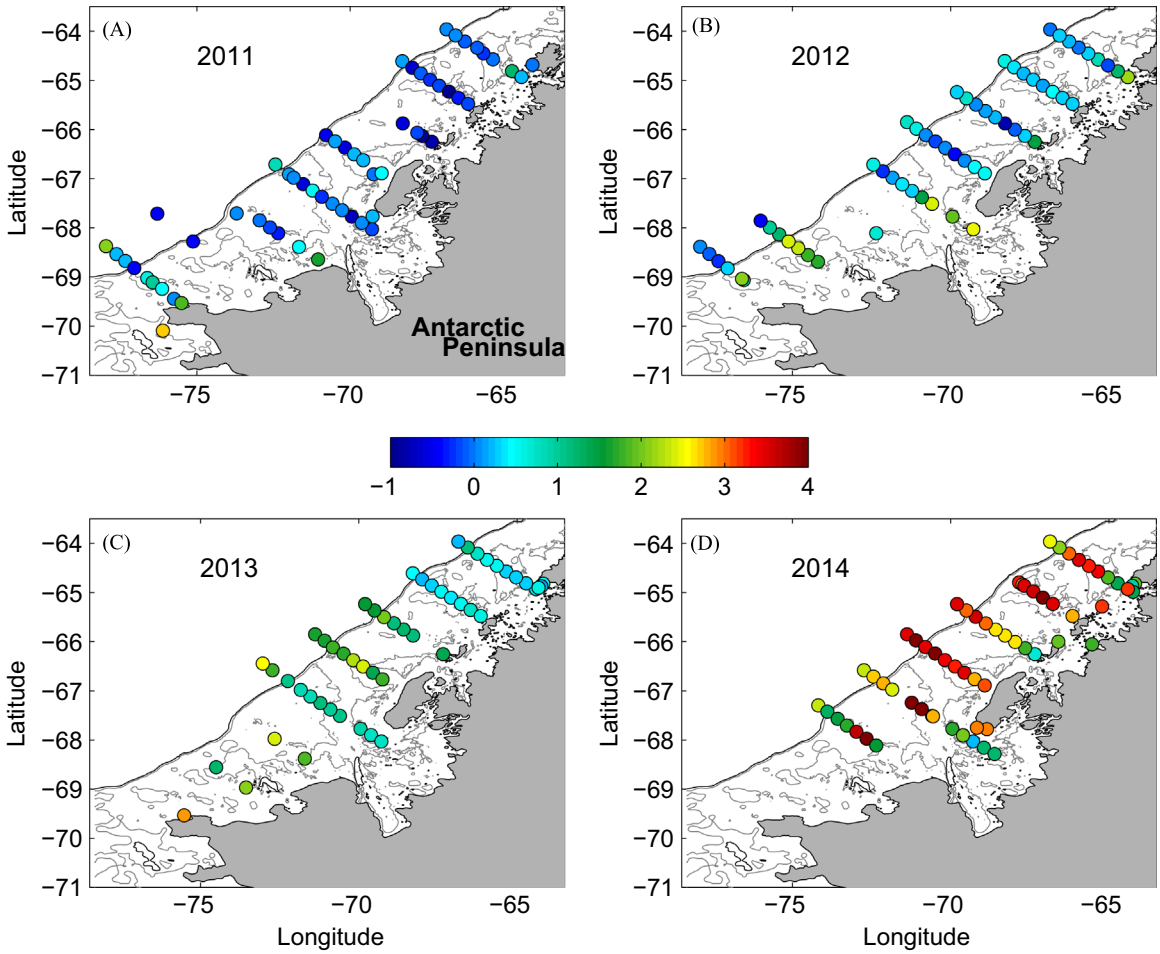

Fig. 4. As per Fig. 2, but for sea ice melt percentage calculated from salinity and $\delta^{18}O$ using Eq. (1). Negative values denote net sea ice formation had occurred from the water sampled.

water prevalence in the nearshore regions in January 2013 (Fig. 5c).

In the final year sampled (2014; Fig. 5d), there was some evidence of nearshore elevation of meteoric water percentages being re-established, with values around 3.5–4% being present close to land. Adjacent to Adelaide Island, there was a region of strong meteoric water prevalence.

4.5. Progression of freshwater properties in $\delta^{18}O$-salinity space

When viewed in $\delta^{18}O$-salinity space (Fig. 6), the near-surface waters show marked differences between the years that reflect the different processes that control the freshwater budget. In January 2011 (Fig. 6a) the core of the surface waters lay along the mixing line between CDW and meteoric water, reflecting the role of CDW as the source oceanic water mass in the region with the bulk of freshening that year being due to strong injections of meteoric water. Deviations from this diagonal mixing line were of the form that the data points were shifted to the right (more saline) in the northern end of the grid, and to the left (less saline) at the southern end of the grid (Fig. 6a). Since these horizontal deviations in salinity-$\delta^{18}O$ space are indicative of sea ice processes, Meredith et al. (2013) inferred that there had been a net southward sea ice motion prior to the time of sampling. This pattern of spatially-structured sea ice formation/melt is also discernible in Fig. 4, albeit in a less overt way.

The biggest contrast with January 2011 in our sequence of data is January 2014 (Fig. 6d). In this year, the deviation of near-surface data points from the diagonal CDW-meteoric water mixing line was as extreme at the northern end of the sampling grid as it was in the south. This is indicative of considerably reduced net southward sea ice motion in 2014 compared with 2011, with slightly more sea ice melt having occurred in the mid-to-northern part of the grid than in the south. The intervening two years (2012, Fig. 6b and 2013, Fig. 6c) were intermediate between the two, though with 2012 showing more resemblance with 2011, and 2013 showing more resemblance with 2014.

4.6. Vertical structure of the freshwater changes

In addition to the surface distributions shown above, the CTD/Niskin bottle profiles that were collected allow changes in the vertical structure of the freshwater distributions to be assessed. There were comparatively few station positions that were sampled in each of the 4 years considered here, nonetheless data from the stations that were sampled in this way indicate that the surface changes are, in general, reliable indicators of the freshwater structure of the underlying ocean also. This is as expected given the freshwater we are examining is buoyant compared with the general water column structure, and its signals are usually maximal at the very surface.

As an example station, Fig. 7 shows the vertical structure of the water column at location 400.100 on the Pal-LTER grid, a mid-shelf location due north of Adelaide Island. The salinity profiles (Fig. 7a) show similar structure below approximately 50 m depth; above this level, the high salinity in January 2011 is clear, as is the very

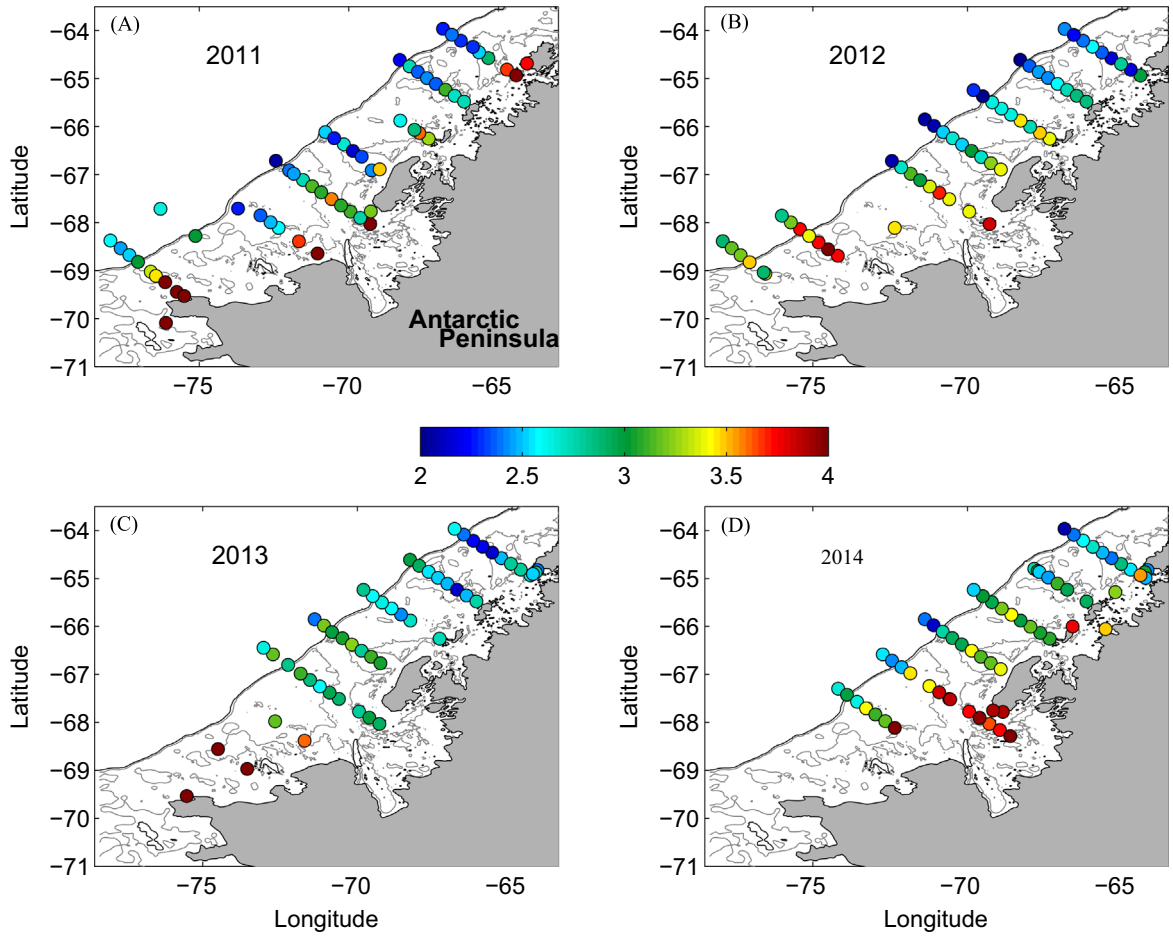

Fig. 5. As per Fig. 2 but for meteoric water percentage calculated from salinity and $\delta^{18}O$ using Eq. (1).

fresh surface layer in January 2014, with 2012 and 2013 lying intermediate between these. When combined with the corresponding measurements of $\delta^{18}O$ (Fig. 7b), profiles of sea ice melt (Fig. 7c) and meteoric water (Fig. 7d) are obtained. Sea ice melt shows a clear maximum (over 2%) at the surface in January 2014, intermediate values in 2013 (around 1% at the surface), and much lower (negative) values in 2011 and 2012. Meteoric water profiles show higher values than sea ice melt in general, with the exception of January 2014 when the high sea ice melt percentage at the surface was comparable to the meteoric water percentage present at that time.

4.7. Rothera time series data

The cruise-based datasets outlined above give comprehensive shelf-wide depictions of the freshwater structure of the WAP, however there is inevitably a question concerning potential aliasing of sub-annual variability and the level to which once-per-year snapshots genuinely depict interannual change. There is thus benefit also in high temporal resolution sampling, so that sub-annual changes can be fully resolved, and the timing of the cruises placed in the context of seasonal and other variability. Fig. 8 shows the updated series of salinity, $\delta^{18}O$ and freshwater concentrations from the RaTS site in Ryder Bay (Fig. 1b). It was also demonstrated previously that year-to-year variability in SAM and ENSO (and, relatedly, winds at the WAP) were reflected in the RaTS series of sea ice melt and meteoric water, particularly when positive SAM coincided with La Niña or negative SAM coincided with El Niño, under which conditions the atmospheric circulation anomalies were especially pronounced (Meredith et al., 2010).

On long (decadal) timescales, it is clear from these series that there has been a general rise in $\delta^{18}O$ (Fig. 8b), and a concurrent decrease in the concentration of meteoric water (Fig. 8d). It was demonstrated previously that this is caused by a progressive deepening of the upper mixed layer at RaTS, which causes freshwater injected at the surface to be spread over a greater vertical interval, and hence diminishes the concentration at the fixed 15 m sampling depth (Meredith et al., 2013). This is still perceived to be a key process in determining the long-term changes at the RaTS site, given the potential for enhanced vertical mixing in the near-coastal environment (Wallace et al., 2008).

The timing of the four Pal-LTER cruises is shown as red bars in Fig. 8a. It can be seen that, at RaTS, January 2011 was the most saline of these, and January 2014 the freshest, with the other two years showing intermediate values. This is the same temporal pattern as is seen in the cruise data (Fig. 2). Similarly, Fig. 8c shows that January 2011 had the lowest sea ice melt concentrations of the 4 years (around 0%), and January 2014 had the highest (more than 2%), again consistent with the temporal pattern in the cruise data (Fig. 4). Indeed, January 2014 is notable in the RaTS series for having the record-length maximum in sea ice melt (close to 3%), exceeding the previous maximum that occurred in early 2005 and 2006 (Fig. 8).

The meteoric water percentages at RaTS at the times of the Pal-LTER cruises show comparatively low values in January 2014 (around 3–3.5%), with marginally higher values in other years (approximately 4% in January 2011, 2012 and 2013). Unlike sea ice melt, this temporal pattern differs from the large-scale pattern seen in the cruise data, which showed a pronounced maximum in meteoric water close to the south side of Adelaide Island in

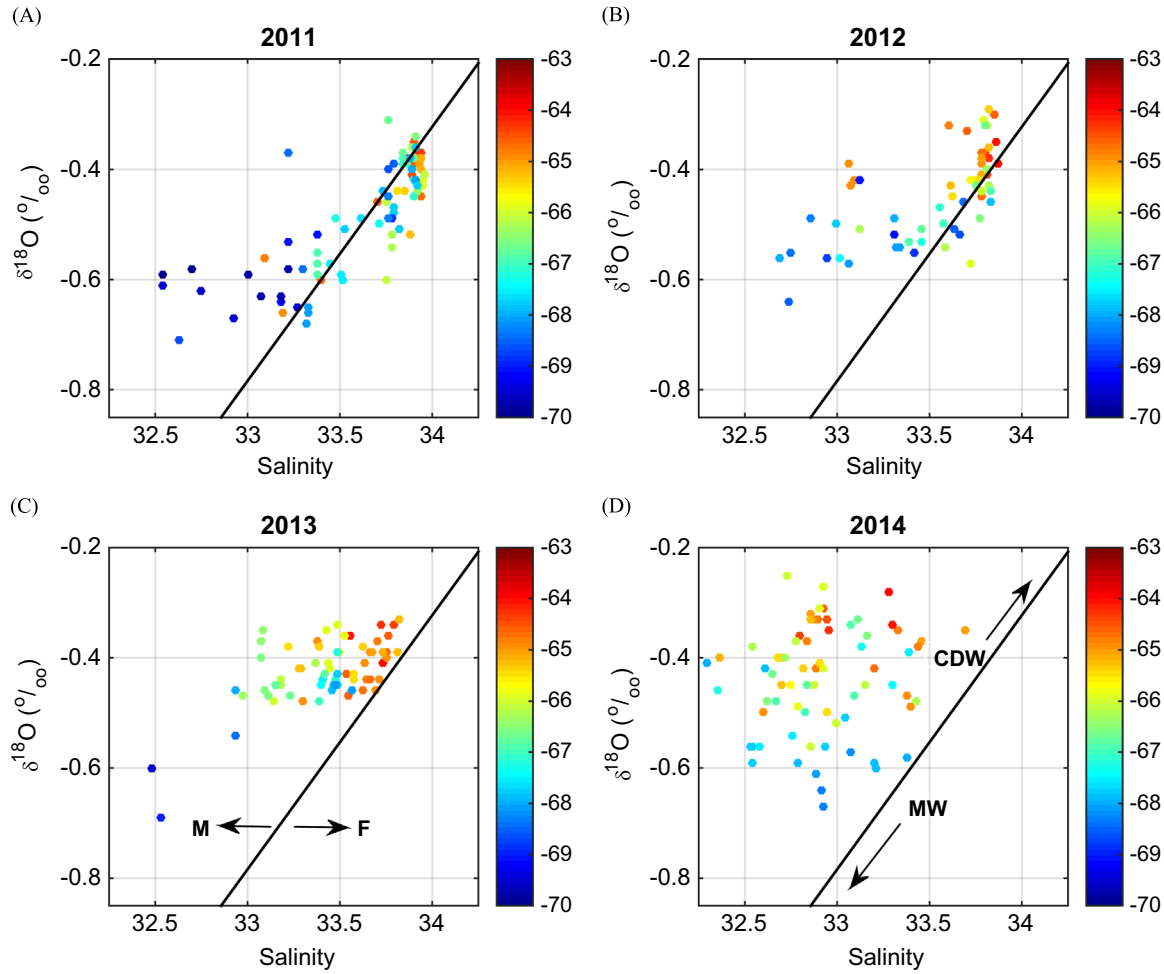

Fig. 6. Near-surface waters of the WAP shelf viewed in δ^{18}O-salinity space for (a) 2011, (b) 2012, (c) 2013 and (d) 2014. Data points are colour-coded by latitude. The diagonal line represents the meteoric water/CDW mixing line: increasing the percentage of CDW in the waters sampled would move the locus of points diagonally up to the right, whereas inclusion of more meteoric water would move the locus of points downward to the left (arrows CDW and MW respectively in panel (d)). By contrast, melting and freezing would move the locus of data points almost horizontally to the left and right respectively (arrows M and F in panel (c)).

January 2014, and an absence of inshore elevation of meteoric water percentages in January 2013.

5. Controls on freshwater distribution changes

5.1. Sea ice changes

The most pronounced signal in the sea ice melt distributions is the progressive change from comparatively low percentages across most of the grid in January 2011 to much higher percentages in January 2014, with intermediate values in years between (Fig. 4). To elucidate the causes of these signals, we here examine the remotely-sensed series of satellite-derived sea ice concentration and extent, in conjunction with wind data for the same period (Fig. 9). Concurrent with the change in sea ice melt distribution is a change from strong net southward winds and sea ice motion prior to the cruise in January 2011, to weak or net northward winds and sea ice motion before the cruise in January 2014. Sea ice motion datasets are available but do not currently span our full period of *in situ* data coverage, however it is known that sea ice in the WAP region (away from the coast) can drift freely and will move at approximately 3% of the surface wind speed and 20–25° to the left of the surface wind direction (Martinson and Wamser, 1990). Thus, when winds are strongly persistently in the southward direction on monthly time scales, this will result in net south-eastward movement of the pack ice; similarly when winds are strongly persistent in the northward direction, this will result in net north-westward movement of the pack ice (Stammerjohn et al., 2003).

Fig. 9a shows that in September 2010, the outermost edge of the ice field was close to its climatological mean for that month, but that marked southward wind anomalies persisted through to November 2010. These resulted in strong southward advection of sea ice, and hence reduced sea ice extent relative to its climatological mean across most of the WAP shelf region. This is manifested as a short sea ice duration and early sea ice retreat relative to the other years of data coverage (Fig. 10).

The following year, northward wind anomalies in September veered to southward wind anomalies during October to December 2011 (Fig. 9b), which pushed the ice edge back more rapidly than the mean climatological retreat for those months, though not to the same extent as seen the previous year. Peak winter sea ice was the highest during our sequence of data, with a later ice edge retreat than in 2010 (Fig. 10).

In 2012, ice extent was low at the ice maximum in August, however wind anomalies were persistently northward from October through to December (Fig. 9c) resulting in a delayed or stalled ice edge retreat and longer ice season duration (Fig. 10) relative to 2010 and 2011. However, the following year, ice extent was high during the peak of winter (Fig. 10), and northward wind anomalies persisted from October through to December (Fig. 9d)

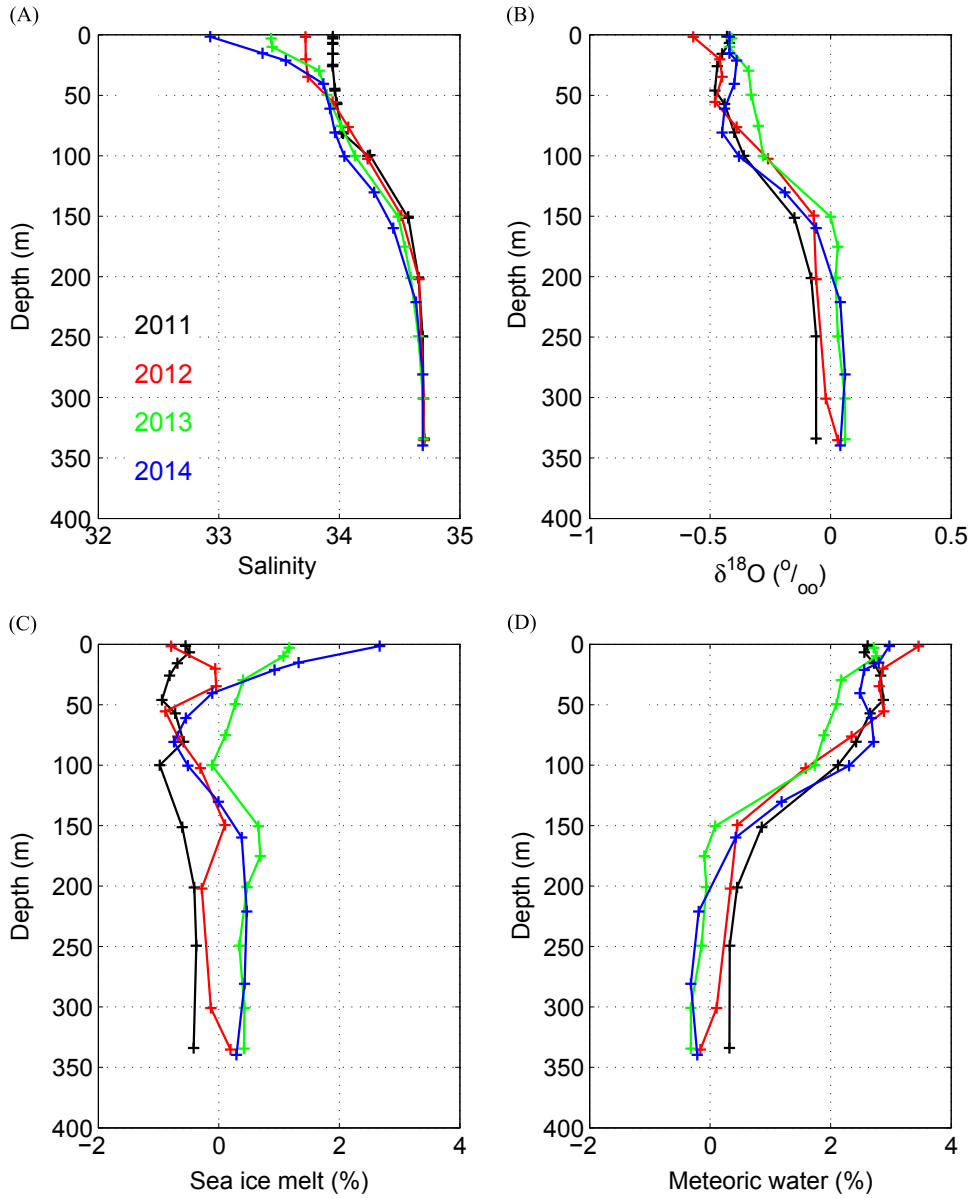

Fig. 7. Vertical profiles of: (a) salinity, (b) $\delta^{18}O$, (c) sea ice melt and (d) meteoric water from location 400.100 (65°52.6′S; 68°17.0′W; due north of Adelaide Island, Fig. 1). Profiles are colour-coded by year, according to the legend in panel (a). Differences from zero in the deeper levels in panels (c) and (d) are less than the uncertainty in the derived freshwater fractions.

resulting in a longer ice season duration and a longer delay in the spring ice edge retreat relative to 2012. The delayed or stalled ice edge retreat results from northward wind anomalies imparting weak northward ice motion inside the ice edge. The stalling of the ice edge occurs because any ice advected northward into solar-warmed waters melts, thus holding the ice edge in place. Under these divergent conditions, the pack ice south of the ice edge also opens up, thus allowing more *in situ* melt to occur there as well. The end result is relatively more ice melting *in situ* in the mid to northern grid, particularly in the summer of 2014 compared to the summer of 2011.

To summarize the salient features of this series:

- 2010: Strong southward wind anomalies caused reduced sea ice extent, resulting in a short ice season duration and an early spring ice edge retreat.
- 2011: Peak sea ice extent was high, with a long ice season duration and late spring ice edge retreat, partially moderated by southward wind anomalies that persisted from October to December.
- 2012: Peak sea ice extent was low, but strong northward wind anomalies during October to December resulted in a long ice season duration and the second latest spring ice edge retreat.
- 2013: Peak sea ice extent was high, and northward wind anomalies during October to December caused a long ice season duration and the latest spring ice edge retreat.

From this pattern of sea ice progression, it is clear that the $\delta^{18}O$-derived fields of sea ice melt are not predominantly controlled by the maximum sea ice extent the preceding winter, although this will inevitably be a factor. For example, the lowest values for $\delta^{18}O$-derived sea ice melt in our sequence (January 2011) were not preceded by the lowest peak winter sea ice extent, which instead occurred in 2012. Also the high sea ice extent in winter 2011 was followed by relatively low percentages of sea ice melt across the WAP shelf in January 2012.

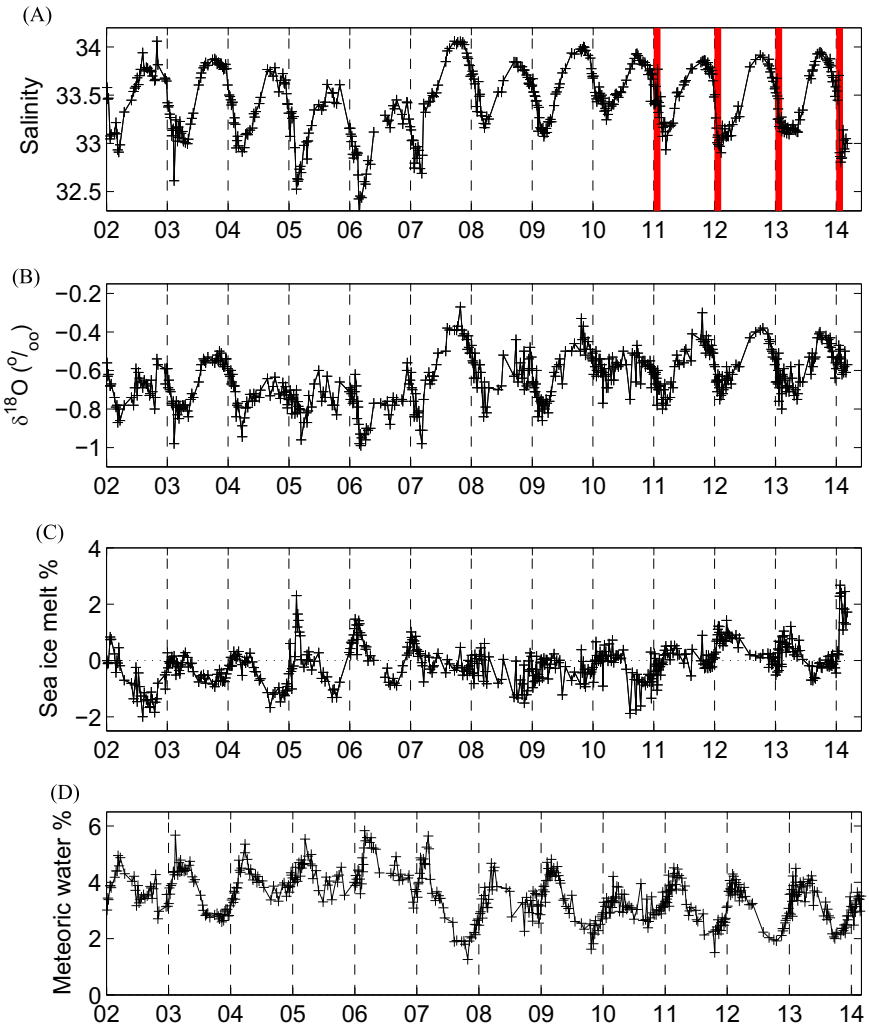

Fig. 8. (a) Salinity, (b) $\delta^{18}O$, (c) sea ice melt and (d) meteoric water from 15 m depth at the Rothera Time Series. Location is marked in Fig. 1b. The timing of the four Pal-LTER cruises used here are marked as vertical red bars in panel (a). (For interpretation of the references to colour in this figure legend, the reader is referred to the web version of this article.)

Instead, it appears that the $\delta^{18}O$-derived fields of sea ice melt depend more directly on the timing of the spring ice edge retreat and (inherently related) the wind-forced sea ice motion. This relationship could be partially caused by the time lag between the ice retreat and the timing of the $\delta^{18}O$ samples being drawn, with longer lags meaning that more net advection and lateral mixing of sea ice melt away from the sampling area will have occurred. Probably more important, however, will be the nature of the wind-forced ice advection, with southward wind anomalies favouring ice advection to the southern end of the sampling grid, and hence earlier ice retreat, with the converse being true for northward wind anomalies. In this context, it should be noted that the earliest retreat (in 2010) occurred before the lowest $\delta^{18}O$-derived sea ice melt values were measured (January 2011), and the latest retreat (2013) occurred before the highest $\delta^{18}O$-derived values were measured (January 2014), with the other years being intermediate in nature between these two extremes.

It should also be noted that this pattern fits very well with the sequence of inferred net sea ice motion in the of $\delta^{18}O$-salinity data (i.e., Fig. 6). We inferred significant southward sea ice motion prior to our sampling in January 2011, from observations of $\delta^{18}O$-derived sea ice formation in the northern grid and melt in the south. In practice, southward wind anomalies in spring and into summer are associated with the transport of sea ice from the northern grid into the southern grid via southward advection, which causes a surplus (deficit) of sea ice melt in the south (north) relative to the amount of sea ice that was initially grown in that area. When we seasonally integrate these effects we detect net sea ice melt in the south and net sea ice production in the north, as indicated in Fig. 6a and to a lesser degree, Fig. 6b. Conversely, northward wind anomalies appear to hold the ice edge further north thus allowing *in situ* melting to occur both in the northern and southern grid, with the imprints of these signals detectable in the $\delta^{18}O$ and salinity tracer fields (Fig. 6d).

It is well known that the meridional winds at the WAP are markedly dependent on SAM and ENSO (e.g. Clem and Fogt, 2013 etc.). Relevant to our data, we note that 2010 was the strongest SAM event on record, coinciding with a strong La Niña event to give very low WAP sea level pressures and resulting in the strong southward winds that were then present. The observed profound impact that this had on the sea ice melt distribution is further evidence of the strong climatic dependence of the WAP freshwater system.

Whilst our time series site at Rothera is close to land and hence not necessarily representative of the broader WAP shelf in all variables measured, we noted above that the sea ice melt derived from the RaTS $\delta^{18}O$ and salinity data show the same temporal pattern as do the four cruises (Fig. 8), with the lowest sea ice melt concentrations present in 2011 (around 0%) and the highest in 2014 (more than 2%; a record-length peak for the series that

exceeded the previous maxima in 2005 and 2006). To examine this in a longer-term context, Fig. 11 shows the sequence of satellite-derived ice season duration for three coastal locations, including adjacent to Adelaide Island. The decadal decrease in each of the series is readily apparent, consistent with the well-known atmospheric warming and sea ice loss at the WAP (Stammerjohn et al., 2008a). Relative to these declining trends, however, it is apparent that 2005 and 2013 were temporal maxima in sea ice duration. These are the winters that precede the peaks in sea ice melt concentrations in the RaTS data, suggesting that the relationship between sea ice melt and ice season duration, as inferred from the cruise data above, is also likely robust over longer periods. This also further reinforces the apparent representativeness of the sea ice melt values at RaTS over larger areas, since the changes in sea ice duration at Adelaide Island is markedly similar to those both north (Anvers Island) and south (Charcot Island) along the WAP coast (Fig. 11).

5.2. Meteoric water changes

Potentially the most significant signal in the sequence of meteoric water distributions in the four Pal-LTER cruises (Fig. 5) is the low values observed in the inshore region in 2013 compared with other years. In 2011, the concentrations of meteoric water were elevated inshore, with particularly high values near Anvers, Adelaide, Alexander and Charcot Islands. In 2012, the concentrations in those areas were somewhat lower, but still elevated compared with concentrations offshore. In 2013, across most of the grid from Anvers Island to Marguerite Bay, concentrations were as high across the open shelf as they were nearshore, though with high concentrations remaining in the vicinity of Charcot Island. In 2014, higher inshore concentrations had been re-established in most locations, especially close to Adelaide Island.

When attributing such signals, and in particular the reduced nearshore concentrations in 2013, it is important to establish whether changes in the near-surface concentrations being examined are indicative of changing freshwater inputs, or instead are due to changes in the vertical distribution of the freshwater after it has entered the ocean. This is especially important given that the decadal decline in near-surface meteoric water concentrations at RaTS has been demonstrated to be caused by a deepening of the mixed layer there, acting to distribute the meteoric water over a greater vertical depth range (Meredith et al., 2013).

To do this, we have examined vertical column integrals of meteoric water from the repeat CTD/Niskin bottle casts undertaken during the cruise (e.g. Fig. 7), calculated as per Meredith et al. (2013). Whilst they are necessarily spatially sparse compared with the near-surface data (which include also data from underway sampling), they do indicate that the anomalously low nearshore meteoric water concentrations in January 2013 were indeed reflective of changes in the total meteoric water column, rather than changes in mixed layer depth, with typically around 1 m less meteoric water being present in 2013 compared with other years. We have also examined depth of the winter mixed layer inferred from the CTD data and calculated as per Martinson et al. (2008), and this too indicated that changes in mixed layer depth were not the cause for the anomalous 2013 results, with winter mixed layers in the nearshore region in 2013 being no deeper than in other years during our sequence of data.

We thus seek an explanation for the anomalously low nearshore meteoric water concentrations in 2013 in terms of reduced input of freshwater instead of changes in its vertical distribution once it has entered the ocean. Glacial melt is a significant contributor to the

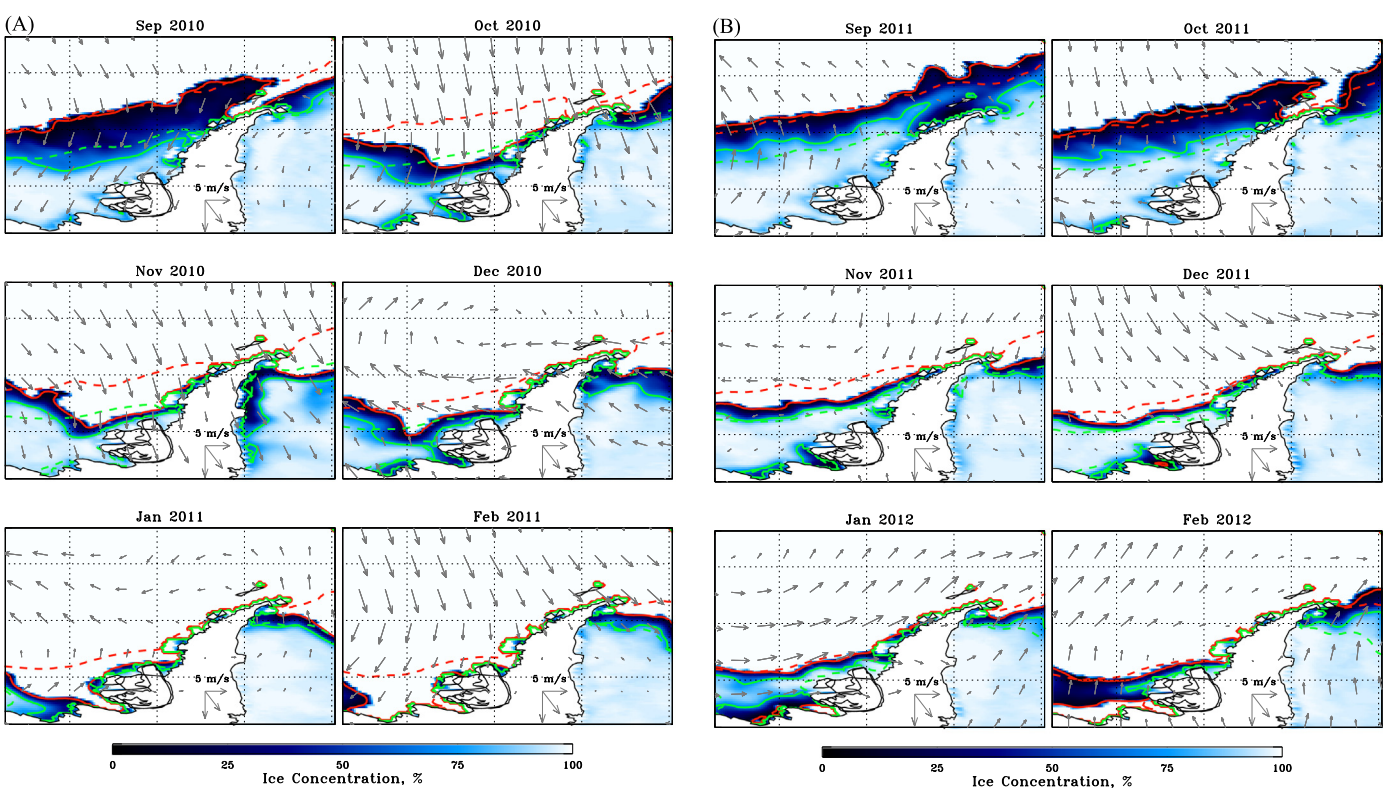

Fig. 9. (a) Sea ice concentration fields for September 2010–February 2011, with wind anomaly vectors overlain (anomalies relative to 1979–2012 mean; scale arrow is shown in each panel). The 15% ice concentration contour is marked in red for the month in question (solid) and for the climatological mean (1979–2012) for that month (dashed). The 75% ice concentration contours are similarly marked, but in green. (b) As for (a), but for September 2011–February 2012. (c) As for (a), but for September 2012–February 2013. (d) As for (a), but for September 2013–February 2014. (For interpretation of the references to colour in this figure legend, the reader is referred to the web version of this article.)

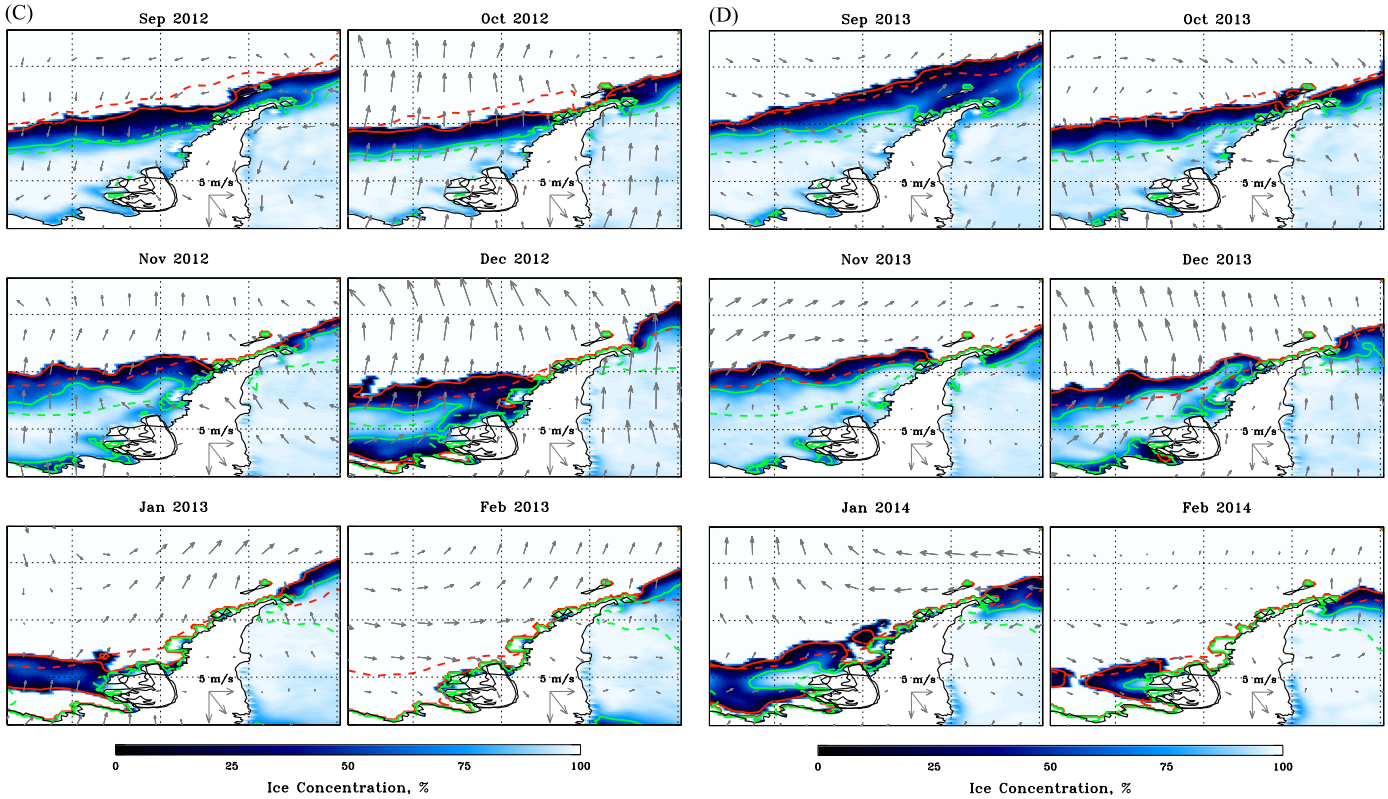

Fig. 9. (*continued*)

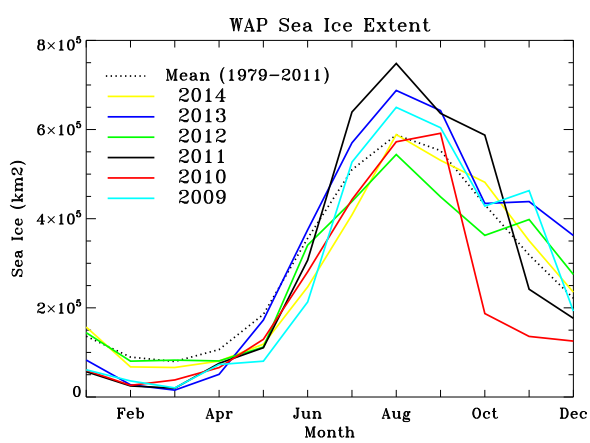

Fig. 10. Sea ice extent at the WAP covering the period 2009–2014, colour-coded by year. For reference, the mean for 1979–2011 is marked (dotted).

meteoric water distribution at the WAP, with different sources potentially contributing (basal melt from ice shelves, runoff of freshwater from the surface and the fronts of marine terminating glaciers, iceberg melt etc). It is not possible to quantitatively assess each of these individually, since the requisite data are not available, however we have assessed PDDs in the context of them being potentially indicative of atmospherically-induced glacial melt. The pattern of PDD is such that comparatively high values occurred in 2010/11 (more than 140 Kd at Rothera station), but then declined through to 2013/14 (less than 60 Kd). Values for 2012/13, prior to the anomalously low meteoric water on the Pal-LTER cruise, were higher, at around 110 Kd. This pattern is repeated across the other WAP stations for which data exist, and indicates that the anomalously low meteoric water concentrations observed in January 2013 were not caused by a decrease in atmospherically-induced glacial melt.

Instead, it seems likely that changes in precipitation were the cause of the signal observed. Fig. 12 shows mean precipitation from RACMO2.3 for the last quarter of each year in the interval 2010–2013, i.e. the three full months preceding each of the cruises. Precipitation values are high over the Peninsula ice sheet, due to orographic effects induced by the chain of mountains along its spine, and are typically elevated over the ocean as well. The last quarters of 2010 and 2011 exemplify this pattern, however the last quarter of 2012 is marked by much lower rates of precipitation both over the Peninsula ice sheet and over the adjacent ocean to the west. In the last 3 months of 2013, precipitation values were higher once more, though not at the same levels as in 2010 or 2011.

It is highly unlikely that the changing precipitation over the Peninsula glaciers during these years had a direct effect on the distribution of meteoric water observed in the Pal-LTER cruises. An illustrative calculation can be used to derive a very approximate timescale for precipitation changes to influence glacial discharge, by relating accumulation rates to ice sheet thickness. If the former were of order 0.5 m per year, and the latter were of order 1000 m (approximate values for Palmer Land), the residence time for ice within the glacial system would be around two millennia. Whilst changes close to shore could occur much more rapidly than this, and regions with higher accumulation and/or a thinner ice sheet will have different residence times, it still seems highly unlikely to be a direct cause of our meteoric water distributions in the ocean. In effect, the Peninsula ice sheet applies a low pass filter to the changes in precipitation it receives that is of sufficient length that interannual changes in outflow are suppressed. Instead, it is precipitation changes over the ocean itself (Fig. 12) that we perceive to be the major direct cause of the changes in ocean meteoric water distributions during our sequence of data.

One consequence of the low inshore meteoric water concentrations in 2013 was that concentrations of sea ice melt there became comparable in magnitude (Fig. 5, cf. Fig. 4). This is counter

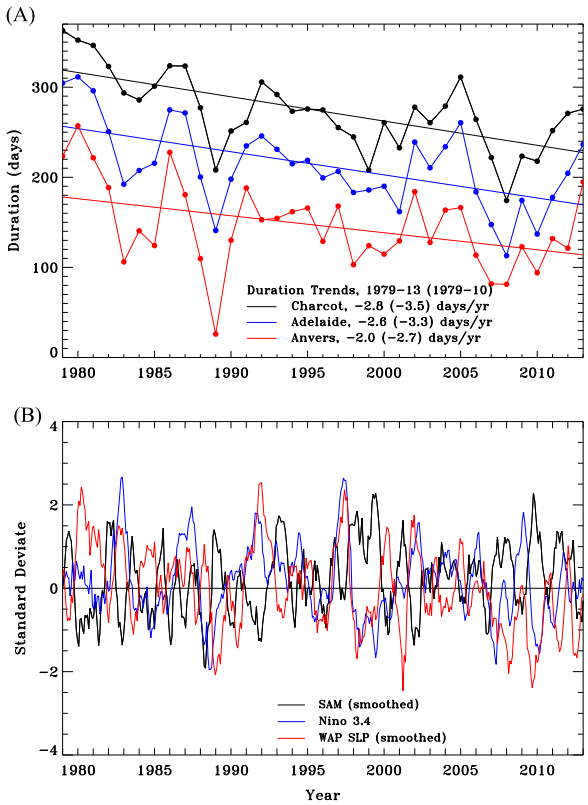

Fig. 11. (a) Annual ice season duration changes for coastal areas adjacent to (black) Charcot Island, (blue) Adelaide Island and (red) Anvers Island. Locations are marked on Fig. 1. (b) Monthly time series of the (smoothed) SAM index (black), Niño 3.4 index (blue) and (smoothed) WAP sea level pressure (SLP; red) over 1979–2013. The SAM and WAP SLP were smoothed with a 7-month running mean filter. All time series are monthly anomalies normalized by the standard deviation. (For interpretation of the references to colour in this figure legend, the reader is referred to the web version of this article.)

to inferences made solely from the first year of cruise data (Meredith et al., 2013), where meteoric water was identified as the dominant freshwater source across the whole WAP shelf. Whilst this may be true for most years, it is clear that this is not always the case. Despite meteoric water concentrations being higher in January 2014 than 2013, sea ice melt concentrations were also much higher, so once more these different components contributed comparable amounts to the overall freshwater budget.

Another consequence is that in 2013, the strong lateral gradients in meteoric water observed previously in the northern part of the grid were not present. These gradients have a marked influence on salinity and hence density, and enhance southward flow in the inner areas of the WAP shelf (Meredith et al., 2013). Increased meteoric water input close to the coast thus has the potential to strengthen the southward geostrophic flow associated with the cross-shelf horizontal density gradients, though the presence of such gradients relies on the meteoric water being the dominant influence on the freshwater distribution at the time in question. From the example of 2013 seen here, however, it is now clear that during years when sea ice melt distributions are very significant (and hence the lateral gradients in salinity may be disrupted), or years when meteoric water input nearshore is very weak, there is an absence of such lateral gradients, with consequences for the magnitude of the southward flows.

As with the sea ice melt distributions, it is the varying winds along the WAP shelf that are perceived to be strongly influencing the meteoric water distributions, albeit via a different mechanism and with different sensitivity. In practice, winds from the north and west at the WAP are typically comparatively warm and moist, being of maritime origin, and hence bring the potential for significant precipitation. By contrast, winds from the south are drier and colder. In this context, we again observe that the SAM reached a record maximum in 2010 that persisted through into 2011, and that a strong La Niña occurred contemporaneously with this, resulting in significant southward wind anomalies. The long-term trend in WAP winds is toward an increase in their southward strength/persistence, associated in particular with a climatic increase in the SAM (Van Wessem et al., 2015). To the extent that this trend may continue, one may thus hypothesize that there could be more frequent occurrences of freshwater distributions like those seen in 2011 in future.

We observe that, unlike for sea ice melt, the temporal progression of the RaTS series of meteoric water concentration does not mimic the cruise data for the overlapping period (Fig. 8). In particular, meteoric water in January 2014 at RaTS appeared lower than the preceding 3 years, most likely reflecting glacial ice changes and precipitation changes associated with local features such as the Sheldon Glacier, and local topographic influences on atmospheric circulation.

At the WAP, sediment cores have been used to reconstruct $\delta^{18}O$ changes on palaeoclimatic timescales, and in some instances have been used to infer changes in glacial ice discharge to the ocean (Pike et al., 2013). The observation made here, of significant variability in seawater $\delta^{18}O$ caused by direct precipitation rather than glacial discharge, combined with the known decadal/centennial trends in WAP precipitation (Thomas et al., 2008), implies significant complexity in the interpretation of such data. Further, the difference in the temporal progression of meteoric water between our time series site and the broader WAP shelf indicate that local proximity to glacial discharge sites can be a significant factor, and hence that the representativeness of the locations of sediment cores needs careful assessment when interpreting their data.

6. Summary and conclusions

In recent decades the Western Antarctic Peninsula changed more rapidly than anywhere else in the Southern Hemisphere, with pronounced consequences for, and feedbacks from, the associated freshwater system. Sea ice has retreated rapidly, and the sea ice season shortened, whilst precipitation has been increasing in the past several decades. Concurrently, there has been a widespread collapse of ice shelves, and an acceleration and retreat of the majority of the glaciers. Indications are that the current trends of glacier melting, recession and thinning are likely to continue throughout the next century.

We have used oxygen isotope and salinity data from research cruises in four consecutive Januaries (2011–2014) to derive new insight into the time-varying, shelf-wide distributions of freshwater from different sources (sea ice melt and meteoric water) at the WAP, and the processes that control them. The distributions of sea ice melt varied greatly between the years, with minima observed in January 2011 rising to maxima in January 2014. Net sea ice motion inferred from the isotope data also varied significantly, with strong southward sea ice motion in 2011, but little or no net ice motion observable by 2014. These changes are linked to shifts in wind forcing, which are themselves strongly influenced by coupled modes of climate variability (SAM and ENSO) that have impacts on meridional winds at the WAP. By comparing with satellite-derived sea ice extent, we find that maximum sea ice extent during the previous winter is not the main direct influence on isotope-derived sea ice melt in summer at the WAP, but that the duration of the sea ice season and the timing of the sea ice retreat are stronger influences.

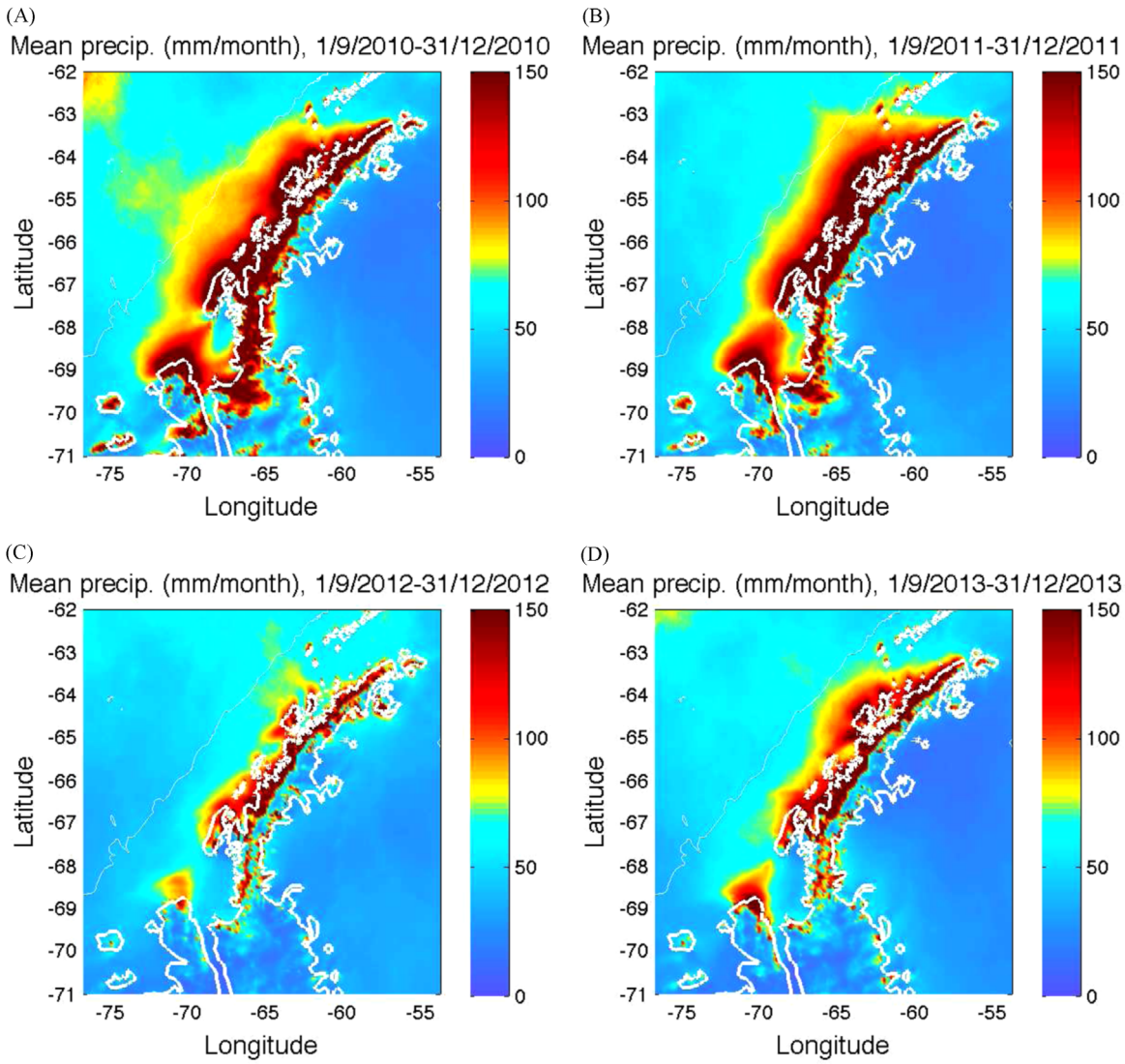

Fig. 12. Mean precipitation for the last 3 months of (a) 2010, (b) 2011, (c) 2012 and (d) 2013, from RACMO2.3.

Meteoric water distributions are also observed to depend on winds, and hence SAM and ENSO, but by different processes and with different sensitivities to sea ice melt. The most noticeable change in the distribution of meteoric water is the absence of high concentrations near-shore at the WAP in January 2013. In previous years, much higher meteoric water prevalence in these areas sustained marked cross-shelf gradients in salinity, influencing lateral density gradients and hence supporting southward geostrophic flows. The absence of the meteoric water in 2013 will thus have an impact on ocean circulation, with consequences for the advection and dispersal of biological material through the WAP region. We have identified the cause of the lower near-shore meteoric water in 2013 to be a reduction in precipitation over the region during the last three months of 2012, which itself was caused by a shift in winds that switched to promote the presence of colder, less moist air masses at the WAP at that time.

Prior to this study, it was thought that meteoric water was the dominant freshwater source across whole WAP shelf, as was the case in the January 2011 cruise data. With the three additional years of cruise data now available, we have seen two examples where sea ice melt concentrations were comparable to meteoric water concentrations: one in January 2013, when the meteoric water concentrations were anomalously low, and one in January 2014, when the sea ice melt concentrations were very high. Whilst the overall change in ocean salinity may not depend strongly on the source from which the freshwater is derived, these sources each have markedly different importance in other variables (e.g. micronutrients), and thus there are potentially significant biogeochemical and ecological consequences to such shifts in relative freshwater contribution.

A near-coastal time series of isotope and salinity data from Rothera Research Station provides longer-term context to the data from the four cruises. We find that the time series data reproduce well the timing of the maxima and minima in sea ice melt seen in the cruise data, illustrating the representativeness of the sampling site as far as this parameter is concerned. In particular, the high January 2014 sea ice melt values seen in the cruise data were contemporaneous with a record-length (> 10 years) maximum in the time series, which exceeded the previous maximum values observed in 2005 and 2006. We note, however, that future climatic changes in the distribution and/or temporal variability of the sea ice at the WAP may change the scale over which the Rothera series is representative. We have recently instigated time series sampling for oxygen isotopes at Palmer Station (Fig. 1a), which will help with future characterisations of this.

Unlike sea ice melt, the meteoric water concentrations in the Rothera time series data did not show significant resemblance to the temporal changes seen in the cruise data. We ascribe this to

local influences, for example the impact of changes in the flow/discharge of the Sheldon Glacier that feeds into Ryder Bay (the time series site), and/or changes in local precipitation. This has potential implications for the interpretation of some climate proxies that are recovered from sediment cores: these are sometimes used to infer seawater $\delta^{18}O$ over millennial timescales, and interpreted in terms of glacial discharge. Our results indicate that careful consideration needs to be given to the location from which such cores are recovered, so that the representativeness of the results over larger-scales can be determined, and so that relative importance of glacial discharge changes versus direct precipitation changes can be addressed. This latter point is reinforced by the observation of greatly reduced near-shore meteoric water in the cruise data in January 2013, which appears to have been caused by weaker precipitation preceding the cruise, rather than a reduction in glacial discharge.

In the longer-term context, the demonstrated sensitivity of both sea ice melt and meteoric water distributions to SAM and ENSO is significant. SAM has been subject to a rising trend in recent decades, due at least partially to anthropogenic effects, and it is predicted that this trend will continue into the future. We note that our 2011 data were collected during a very strong positive SAM event, which also coincided with a strong La Niña. To the extent that such conditions are useful indicators of potential future change, one could speculate that freshwater distributions at the WAP may resemble our 2011 data more frequently in the years to come. In particular, the ongoing shift toward more southward wind anomalies at the WAP could lead to more persistent southward sea ice motion, suppressed sea ice melt percentages, and more frequent occurrences of high meteoric water concentrations near-shore. This latter effect would also act to sustain the southward geostrophic flow on the shelf, and hence the southward export of freshwater and biological material out of the WAP sampling area. Predictions of ongoing increases in glacial melt and discharge over the course of the coming century reinforce this speculation, however it is important that the correct observational data are collected to ensure that any such changes are reliably tracked and attributed, and that their impacts on the regional climate system and ecosystem are identified. Our ongoing isotopic oceanography at the WAP will be central to this effort.

Acknowledgements

We thank the officers, crew and scientists of the ARSV *Laurence M. Gould* for the assistance in collecting the cruise data used here, and the succession of marine assistants at Rothera Research Station for collecting isotope samples and data. We also thank the three reviewers for their insightful comments that helped strengthen this paper. Richard Hindmarsh is thanked for advice relating to glaciology, and Carol Arrowsmith is thanked for the oxygen isotope analysis. The Palmer LTER participants acknowledge NSF Awards 0823101 and PLR-1440435. The RACMO project is funded by the Netherlands Polar Programme (NPP) and the Netherlands Organization of Scientific Research, Earth and Life Sciences section (NWO/ALW), and carried out at IMAU. This paper is a contribution of the BAS Polar Oceans programme, funded by the Natural Environment Research Council.

References

Barrand, N.E., Hindmarsh, R.C.A., Arthern, R.J., Williams, C.R., Mouginot, J., Scheuchl, B., Rignot, E., Ligtenberg, S.R.M., van den Broeke, M.R., Edwards, T.L., Cook, A.J., Simonsen, S.B., 2013a. Computing the volume response of the Antarctic Peninsula ice sheet to warming scenarios to 2200. J. Glaciol. 59, 397–409.

Barrand, N.E., Vaughan, D.G., Steiner, N., Tedesco, M., Kuipers-Munneke, P., van den Broeke, M.R., Hosking, J.S., 2013b. Trends in Antarctic Peninsula surface melting conditions from observations and regional climate modelling. J. Geophys. Res. 118, 315–330.

Beardsley, R.C., Limeburner, R., Owens, W.B., 2004. Drifter measurements of surface currents near Marguerite Bay on the western Antarctic Peninsula shelf during austral summer and fall, 2001 and 2002. Deep-Sea Res. II 51, 1947–1964.

Boyd, P.W., Ellwood, M.J., 2010. The biogeochemical cycle of iron in the ocean. Nat. Geosci. 3, 675–682.

Bracegirdle, T., 2013. Climatology and recent increase of westerly winds over the Amundsen Sea derived from six reanalyses. Int. J. Climatol. 33, 843–851.

Cane, M.A., Zebiak, S.E., Dolan, S.C., 1986. Experimental forecasts of El Niño. Nature 322, 827–832.

Clarke, A., Meredith, M.P., Wallace, M.I., Brandon, M.A., Thomas, D.N., 2008. Seasonal and interannual variability in temperature, chlorophyll and macronutrients in Ryder Bay, northern Marguerite Bay, Antarctica. Deep-Sea Res. II 55, 1988–2006.

Clem, K.R., Fogt, R.L., 2013. Varying roles of ENSO and SAM on the Antarctic Peninsula climate in austral spring. J. Geophys. Res. 118, 11481–11492.

Comiso, J., 2002. Bootstrap sea ice concentrations from Nimbus-7 SMMR and DMSP SSM/I-SSMIS, Version 2. National Snow and Ice Data Center, Boulder, CO http://www.nsidc.org/data/nsidc-0079.html.

Comiso, J.C., Nishio, F., 2008. Trends in the sea ice cover using enhanced and compatible AMSR-E, SSM/I, and SMMR data. J. Geophys. Res., 113.

Cook, A.J., Fox, A.J., Vaughan, D.G., Ferrigno, J.G., 2005. Retreating glacier fronts on the Antarctic Peninsula over the past half-century. Science 308, 541–544.

Craig, H., Gordon, L., 1965. Deuterium and oxygen-18 variations in the ocean and the marine atmosphere. In: Tongiorgio, E. (Ed.), Stable Isotopes in Oceanographic Studies and Paleotemperatures, pp. 9–130.

Davies, B.J., Golledge, N.R., Glasser, N.F., Carrivick, J.L., Ligtenberg, S.R.M., Barrand, N. E., van den Broeke, M.R., Hambrey, M.J., Smellie, J.L., 2014. Modelled glacier response to centennial temperature and precipitation trends on the Antarctic Peninsula. Nat. Clim. Change.

Dee, D.P., Uppala, S.M., Simmons, A.J., Berrisford, P., Poli, P., Kobayashi, S., Andrae, U., Balmeseda, M.A., Balsamo, G., Bauer, P., Bechtold, P., Beljaars, A.C.M., van den Berg, L., Bidlot, J., Bormann, N., Delsol, C., Dragani, R., Fuentes, M., Geer, A.J., Haimberger, L., Healy, S.B., Hersbach, H., Holm, E.V., Isaksen, L., Kallberg, P., Kohler, M., Matricardi, M., McNally, A.P., Monge-Sanz, B.M., Morcrette, J.-J., Park, B.-K., Peubey, C., Rosnay, P., Tavolato, C., Thepaut, J.-N., Vitart, F., 2011. The ERA-Interim reanalysis: configuration and performance of the data assimilation system. Q. J. R. Meteorol. Soc. 137, 553–597.

Dierssen, H.M., Smith, R.C., Vernet, M., 2002. Glacial meltwater dynamics in coastal waters west of the Antarctic Peninsula. Proc. Natl. Acad. Sci. 99, 1790–1795.

Ducklow, H.W., Clarke, A., Doney, S.C., Geisz, H., Martinson, D.G., Meredith, M.P., Montes-Hugo, M., Schofield, O., Stammerjohn, S.E., Steinberg, D., Fraser, W., 2012. Marine pelagic ecosystems: the west Antarctic Peninsula. In: Rogers, A.D., Murphy, E.J., Johnston, N.M., Clarke, C. (Eds.), Antarctica: An Extreme Environment in a Changing World. John Wiley & Sons, London.

Edwards, R., Sedwick, P., 2001. Iron in East Antarctic snow: Implications for atmospheric iron deposition and algal production in Antarctic waters. Geophys. Res. Lett. 28, 3907–3910.

Epstein, S., Mayeda, T.K., 1953. Variation of ^{18}O content of waters from natural sources. Geochim. Cosmochim. Acta 4, 213–224.

Fogt, R.L., Bromwich, D.H., 2006. Decadal variability of the ENSO teleconnection to the high latitude South Pacific governed by coupling with the Southern Annular Mode. J. Clim. 19, 979–997.

Harangozo, S., 2006. Atmospheric circulation impacts on winter maximum sea ice extent in the west Antarctic Peninsula region (1979–2001). Geophys. Res. Lett., 33. http://dx.doi.org/10.1029/2005GL024978.

Hawkings, J.R., Wadham, J.L., Tranter, M., Raiswell, R., Benning, L.G., Stathan, P.J., Tedstone, A., Nienow, P., Lee, K., Telling, J., 2014. Ice sheets as a significant source of highly reactive nanoparticulate iron to the oceans. Nat. Commun. 5.

Jullion, L., Naveira Garabato, A.C., Meredith, M.P., Holland, P.R., Courtois, P., King, B. A., 2013. Decadal freshening of the Antarctic Bottom Water exported from the Weddell Sea. J. Clim. 26, 8111–8125.

King, J.C., 1994. Recent climate variability in the vicinity of the Antarctic Peninsula. Int. J. Climatol. 14, 357–369.

King, J.C., Harangozo, S.A., 1998. Climate change in the western Antarctic Peninsula since 1945: observations and possible causes. Ann. Glaciol. 27, 571–575.

Kirchgäßner, A., 2011. An analysis of precipitation data from the Antarctic base Faraday/Vernadsky. Int. J. Climatol. 31, 404–414.

Klinck, J.M., 1998. Heat and salt changes on the continental shelf west of the Antarctic Peninsula between January 1993 and January 1994. J. Geophys. Res. 103, 7617–7636.

Klinck, J.M., Hofmann, E.E., Beardsley, R.C., Salighoglu, B., Howard, S., 2004. Water mass properties and circulation on the West Antarctic Peninsula continental shelf in austral fall and winter 2001. Deep-Sea Res. II 51, 1925–1946.

Marshall, G.J., 2003. Trends in the Southern Annular Mode from Observations and Reanalyses. J. Clim. 16, 4134–4143.

Marshall, G.J., Orr, A., van Lipzig, N., King, J., 2006. The impact of a changing southern hemisphere annular mode on Antarctic Peninsula summer temperatures. J. Clim. 19, 5388–5404.

Martinson, D.G., 2011a. Antarctic circumpolar current's role in the Antarctic ice system: an overview. Palaeogeogr. Palaeoclimatol. Palaeoecol.

Martinson, D.G., 2011b. Transport of warm upper circumpolar deep water onto the Western Antarctic Peninsula Continental Shelf. Ocean Sci. Discuss. 8, 2479–2502.
Martinson, D.G., Stammerjohn, S.E., Iannuzzi, R.A., Smith, R.C., Vernet, M., 2008. Western Antarctic Peninsula physical oceanography and spatio-temporal variability. Deep-Sea Res. II 55, 1964–1987.
Martinson, D.G., Wamser, C., 1990. Ice drift and momentum exchange in the winter Antarctic ice pack. J. Geophys. Res. 95, 1741–1755.
Maslanik, J.A., Stroeve, J., 1999. Near-Real-Time DMSP SSM/I-SSMIS Daily Polar Gridded Sea Ice Concentrations. National Snow and Ice Data Center, Boulder, CO, USA.
Meredith, M., Brandon, M.A., Wallace, M.I., Clarke, A., Leng, M.J., Renfrew, I.A., van Lipzig, N.P.M., King, J.C., 2008a. Variability in the freshwater balance of northern Marguerite Bay, Antarctic Peninsula: results from $\delta^{18}O$. Deep-Sea Res. II 55, 309–322.
Meredith, M.P., Grose, K.E., McDonagh, E.L., Heywood, K.J., Frew, R.D., Dennis, P.F., 1999. Distribution of oxygen isotopes in the water masses of Drake Passage and the South Atlantic. J. Geophys. Res. 104, 20,949–920,962.
Meredith, M.P., King, J.C., 2005. Rapid climate change in the ocean west of the Antarctic Peninsula during the second half of the 20th century. Geophys. Res. Lett. 32, 1–5.
Meredith, M.P., Murphy, E.J., Hawker, E.J., King, J.C., Wallace, M.I., 2008b. On the interannual variability of ocean temperatures around South Georgia, Southern Ocean: forcing by El Niño/Southern Oscillation and the Southern Annular Mode. Deep-Sea Res. II 55, 2007–2022.
Meredith, M.P., Renfrew, I.A., Clarke, A., King, J.C., Brandon, M.A., 2004. Impact of the 1997/98 ENSO on the upper waters of Marguerite Bay, western Antarctic Peninsula. J. Geophys. Res., 109. http://dx.doi.org/10.1029/2003JC001784.
Meredith, M.P., Venables, H.J., Clarke, A., Ducklow, H., Erickson, M., Leng, M.J., Lenaerts, J.T.M., van den Broeke, M.R., 2013. The freshwater system west of the Antarctic Peninsula: spatial and temporal changes. J. Clim. 26, 1669–1684.
Meredith, M.P., Wallace, M.I., Stammerjohn, S.E., Renfrew, I.A., Clarke, A., Venables, H.J., Shoosmith, D.R., Souster, T., Leng, M.J., 2010. Changes in the freshwater composition of the upper ocean west of the Antarctic Peninsula during the first decade of the 21st century. Prog. Oceanogr. 87, 127–143.
Mitchell, B.G., Holm-Hansen, O., 1991. Observations and modeling of the Antarctic phytoplankton crop in relation to mixing depth. Deep-Sea Res. 38, 981–1007.
Moffat, C., Beardsley, R., Owens, W.B., van Lipzig, N., 2008. A first description of the Antarctic Peninsula Coastal Current. Deep-Sea Res. II 55, 277–293.
Moffat, C., Owens, B., Beardsley, R.C., 2009. On the characteristics of Circumpolar Deep Water intrusions to the west Antarctic Peninsula Continental Shelf. J. Geophys. Res. 114, C05017.
Montes-Hugo, M., Doney, S.C., Ducklow, H.W., Fraser, W., Martinson, D., Stammerjohn, S.E., Schofield, O., 2009. Recent changes in phytoplankton communities associated with rapid regional climate change along the western Antarctic Peninsula. Science 323, 1470–1473.
Mosby, H., 1934. The waters of the Atlantic Antarctic Ocean. Scientific Results of the Norwegian Antarctic Expedition 1927–1928 11, 1–131.
Östlund, H.G., Hut, G., 1984. Arctic Ocean water mass balance from isotope data. J. Geophys. Res. 89, 6373–6381.
Pike, J., Swann, G.E.A., Leng, M.J., Snelling, A.M., 2013. Glacial discharge along the west Antarctic Peninsula during the Holocene. Nat. Geosci.
Pritchard, H.D., Ligtenberg, S.R.M., Fricker, H.A., Vaughan, D.G., van den Broeke, M. R., Padman, L., 2012. Antarctic ice-sheet loss driven by basal melting of ice shelves. Nature 484, 502–505.
Pritchard, H.D., Vaughan, D.G., 2007. Widespread acceleration of glaciers on the Antarctic Peninsula. J. Geophys. Res., 112.
Raiswell, R., 2011. Iceberg-hosted nanoparticulate Fe in the Southern Ocean Mineralogy, origin, dissolution kinetics and source of bioavailable Fe. Deep-Sea Res. II 58, 1364–1375.
Reijmer, C.H., van Meijgaard, E., van den Broeke, M.R., 2005. Evaluation of temperature and wind over Antarctica in a Regional Atmospheric Climate Model using 1 year of automatic weather station data and upper air observations. J. Geophys. Res., 110.
Rye, C.D., Garabato, A.C.N., Holland, P.R., Meredith, M.P., Nurser, A.J.G., Hughes, C.W., Coward, A.C., Webb, D.J., 2014. Rapid sea-level rise along the Antarctic margins in response to increased glacial discharge. Nat. Geosci. 7, 732–735.
Saba, G.K., Fraser, W.R., Saba, V.S., Iannuzzi, R.A., Coleman, K.E., Doney, S.C., Ducklow, H.W., Martinson, D.G., Miles, T.N., Patterson-Fraser, D.L., Stammerjohn, S.E., Steinberg, D.K., Schofield, O.M., 2014. Winter and spring controls on the summer food web of the coastal West Antarctic Peninsula. Nat. Commun. 5, 4318.
Savidge, D.K., Amft, J.A., 2009. Circulation on the West Antarctic Peninsula derived from 6 years of ADCP transects. Deep-Sea Res. I 56, 1633–1655.
Scambos, T., Hulbe, C., Fahnestock, M., Bohlander, J., 2000. The link between climate warming and break-up of ice shelves in the Antarctic Peninsula. J. Glaciol. 46, 516–530.
Schlosser, P., Bayer, R., Foldvik, A., Gammelsrod, T., Rohardt, G., Munnich, K.O., 1990. Oxygen 18 and helium as tracers of Ice Shelf Water and water/ice interaction in the Weddell Sea. J. Geophys. Res. 95, 3253–3263.
Schmidtko, S., Thompson, A.F., Aoki, S., 2014. Multidecadal warming of Antarctic waters. Science 346, 1227–1231.
Smith, R.C., Stammerjohn, S.E., 2001. Variations of surface air temperature and sea ice extent in the western Antarctic Peninsula (WAP) region. Ann. Glaciol. 33, 493–500.
Smith, R.C., Stammerjohn, S.E., Baker, K.S., 1996. Surface air temperature variations in the western Antarctic peninsula regions. In: Ross, R.M., Hofmann, E.E., Quetin, L.B. (Eds.), Foundations for Ecological Research West of the Antarctic Peninsula. American Geophysical Union, Washington, DC, pp. 105–121.
Stammerjohn, S.E., Drinkwater, M.R., Smith, R.C., Liu, X., 2003. Ice-atmosphere interactions during sea-ice advance and retreat in the western Antarctic Peninsula region. J. Geophys. Res.—Oceans, 108. http://dx.doi.org/10.1029/2002JC001543.
Stammerjohn, S.E., Martinson, D.G., Smith, R.C., Ianuzzi, R.A., 2008a. Sea ice in the western Antarctic Peninsula region: spatio-temporal variability from ecological and climate change perspectives. Deep-Sea Res. II, 55.
Stammerjohn, S.E., Martinson, D.G., Smith, R.C., Yuan, X., Rind, D., 2008b. Trends in Antarctic annual sea ice retreat and advance and their relation to El Niño-Southern Oscillation and Southern Annular Mode variability. J. Geophys. Res., 113.
Thomas, E.R., Marshall, G.J., McConnell, J.R., 2008. A doubling in snow accumulation in the Western Antarctic Peninsula. Geophys. Res. Lett., 35.
Thompson, D.W.J., Wallace, J.M., 2000. Annular modes in the extratropical circulation. Part I: Month-to-month variability. Jo. Clim. 13, 1000–1016.
Thompson, D.W.J., Wallace, J.M., Hegerl, G.C., 2000. Annular modes in the extratropical circulation. Part II: Trends. J. Clim. 13, 1018–1036.
Tournadre, J., Bouhier, N., Girard-Ardhuin, F., Rémy, F., 2016. Antarctic icebergs distribution 1992–2014. J. Geophys. Res.
Turner, J., 2004. The El Niño-Southern Oscillation and Antarctica. Int. J. Climatol. 24, 1–31.
Turner, J., Colwell, S.R., Harangozo, S., 1997. Variability of precipitation over the coastal western Antarctic Peninsula from synoptic observations. J. Geophys. Res. 102, 13999–14007.
Turner, J., Colwell, S.R., Marshall, G.J., Lachlan-Cope, T.A., Carleton, A.M., Jones, P.D., Lagun, V., Reid, P.A., Iagovinka, S., 2005. Antarctic climate change during the last 50 years. Int. J. Climatol. 25, 279–294.
Turner, J., Maksym, E., Phillips, A., Marshall, G.J., Meredith, M.P., 2013. The impact of changes in sea ice advance on the large winter warming on the western Antarctic Peninsula. Int. J. Climatol. 33, 852–861.
van den Broeke, M.R., 2005. Strong surface melting preceded collapse of Antarctic Peninsula ice shelf. Geophys. Res. Lett., 32.
Van Wessem, J.M., Reijmer, C.H., van de Berg, W.J., van den Broeke, M.R., Cook, A.J., van Ulft, L.H., van Meijgaard, E., 2015. Temperature and wind climate of the Antarctic Peninsula as simulated by a high-resolution atmospheric climate model. J. Clim. 28, 7306–7326. http://dx.doi.org/10.1175/JCLI-D-15-0060.1.
Van Wessem, J.M., Reijmer, C.H., Morlighem, M., Mouginot, J., Rignot, E., Medley, B., Joughin, I., Wouters, B., Depoorter, M.A., Bamber, J.L., Lenaerts, J.T.M., van den Berg, W.J., van den Broeke, M.R., van Meijgaard, E., 2014. Improved representation of East Antarctic surface mass balance in a regional atmospheric climate model. J. Glaciol. 60, 761–770.
Vaughan, D.G., 2006. Recent trends in melting conditions on the Antarctic Peninsula and their implications for ice-sheet mass balance and sea level. Arct. Antarct. Alp. Res. 38, 147–152.
Vaughan, D.G., Marshall, G.J., Connolley, W.M., Parkinson, C., Mulvaney, R., Hodgson, D.A., King, J.C., Pudsey, C.J., Turner, J., 2003. Recent rapid regional climate warming on the Antarctic Peninsula. Clim. Change 60, 243–274.
Venables, H.J., Clarke, A., Meredith, M.P., 2013. Wintertime controls on summer stratification and productivity at the western Antarctic Peninsula. Limnol. Oceanogr. 58, 1035–1047.
Wallace, M.I., Meredith, M.P., Brandon, M.A., Sherwin, T.J., Dale, A., Clarke, A., 2008. On the characteristics of internal tides and coastal upwelling behaviour in Marguerite Bay, west Antarctic Peninsula. Deep-Sea Res. II 55, 2023–2040.
Weiss, R.F., Östlund, H.G., Craig, H., 1979. Geochemical studies of the Weddell Sea. Deep-Sea Res. 26A, 1093–1120.
Yuan, X., 2004. ENSO-Related Impacts on Antarctic Sea Ice: Synthesis of Phenomemon and Mechanisms. Antarct. Sci. 16, 415–425.